DYNAMIC RANGE OF ANALOG FIBER OPTIC LINKS USED IN MICROCELLULAR MOBILE RADIO APPLICATIONS

by

ANISH S.KELKAR

Thesis submitted to the faculty of the
Virginia Polytechnic Institute and State University
in partial fulfillment of the requirements for the degree of
MASTER OF SCIENCE

in

Electrical Engineering

APPROVED

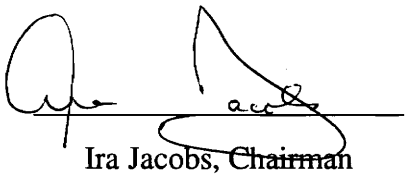

Ira Jacobs, Chairman

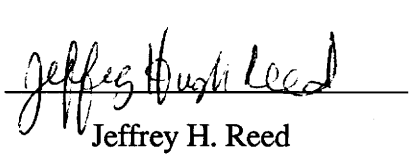

Jeffrey H. Reed

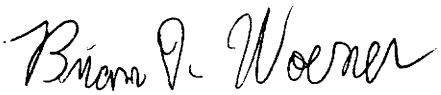

Brian D. Woerner

December 1994

C.2

LD
5655
V855
1994
K455
c.2

DYNAMIC RANGE OF ANALOG FIBER OPTIC LINKS USED FOR MOBILE RADIO APPLICATIONS

Anish Kelkar
Ira Jacobs, Chaiman
Bradley Department of Electrical Engineering
Virginia Polytechnic Institute and State University VA 24060

ABSTRACT

The use of analog fiber optic links for microcellular mobile radio comminications has been the focus of considerable research recently. These systems have the advantages relative to coaxial cable of low noise and enormous bandwidth. Analog subcarrier multiplexing techniques are used for transmitting the mobile signals over the fiber. Use of this technology however presents some unique problems due to the nonlinearities of the fiber optics system and the noise introduced by it. In this thesis, we analyse the dynamic range of the fiber links used for these applications.

The dynamic range is limited by the noise and the nonlinear distortion introduced by the fiber link. The main sources of nonlinear distortion are threshold clipping, gain saturation of the laser, and the combination of laser chirp and fiber dispersion. We have analytically modeled these nonlinearities and used these models to understand the dependence of the nonlinear distortion on the physical parameters of the laser diode and the fiber and also on the modulation index per channel and the number of channels. The performance of the IS-19 AMPS signals and the IS-54 TDMA signals in the presence of fiber link noise is also discussed. Finally, the dynamic range of the fiber link for both AMPS and TDMA signals has been analyzed. The dynamic range of the fiber link is limited by the threshold clipping nonlinearity. It is also highly dependent on the number of mobile signals that are being communicated over the fiber link.

ACKNOWLEDGMENTS

First and foremost, I would like to express my gratitude to Dr. Ira Jacobs. Without his inspiration and guidance this work would not have been completed. I would like to thank Dr. J. H. Reed for his extremely valuable help in this work. Thanks are also due to Dr. B. D. Woerner, not only for his useful comments, but also for being a constant source of encouragement from the day I came to Virginia Tech. This research work was supported by SouthWestern Bell.

Last, but certainly not the least, I would like to thank my parents Mr. Sudhakar Kelkar and Mrs. Sheela Kelkar and my sister, Sejal Kelkar. No words can do justice to the love and affection that they have showered upon me.

TABLE OF CONTENTS

ABSTRACT		ii
ACKNOWLEDGEMENTS		iii
TABLE OF CONTENTS		iv
LIST OF FIGURES		vi
LIST OF TABLES		viii
CHAPTER 1. INTRODUCTION		1
1.1	Review of Wireless Communications	1
1.2	Fiber Optic Links used for Analog Transmission	3
1.3	Architecture of Fiber Optic links used for Wireless Communications Applications	3
1.4	Previous Research	4
1.5	Organization of Thesis	5
CHAPTER 2. NOISE AND NONLINEAR EFFECTS ON ANALOG TRANSMISSION		9
2.1	Nonlinearities in the Fiber Optic Link	9
	2.1.1 Gain Saturation in the Laser Diode	10
	2.1.2 Threshold Clipping	10
	2.1.3 Combination of Laser Chirp and Fiber Dispersion Nonlinearity	12
	2.1.4 Fiber Nonlinearity	13
2.2	Noise in the Fiber Optics system	15
2.3	Summary	17
CHAPTER 3. GAIN SATURATION IN LASER DIODES		22
3.1	Overview of Gain Saturation	22
3.2	Laser Rate Equations	23
3.3	Nonlinear Modeling	25
3.4	Variation of nonlinearity with various physical parameters	31
3.5	Summary	32
CHAPTER 4. DISPERSION AND CHIRP MODELING		43
4.1	Overview of Dispersion and Chirp in AM-SCM systems	43
4.2	Chirp Modeling	44
4.3	Dispersion Modeling	46

4.4 Behavior of the nonlinearity with various physical parameters 50
4.5 Conclusions 52

CHAPTER 5. PERFORMANCE OF MOBILE SIGNALS IN THE PRESENCE OF FIBER LINK NOISE 59

5.1 Noise in AMPS FM signal 59
5.2 BER Analysis for TDMA signals 65
5.3 Numerical Results 66
5.4 Summary 67

CHAPTER 6. DYNAMIC RANGE OF MOBILE SIGNALS

6.1 Dynamic range for the mobile signals 73
6.2 Noise and nonlinear distortion requirements for AMPS and TDMA systems 76
6.3 Dynamic Range results 77
6.4 Summary 79

CHAPTER 7. SUMMARY AND CONCLUSIONS 88

REFERENCES 90

VITA 93

LIST OF FIGURES

Figures

1.1	Intensity modulation of the laser diode	7
1.2	Architecture of the microcellular system using intensity modulated laser	8
2.1	Threshold clipping of laser diode	18
2.2	Third order nonlinear distortion versus rms modulation index μ [23]	19
2.3	Variation of the input threshold power at which SBS degrades the noise performance versus the linewidth enhancing factor of the laser	20
2.4	CNR versus average received power P_0, showing the regions where the receiver thermal noise, shot noise and the laser RIN noise are dominant	21
3.1	Optical gain of a laser diode showing gain saturation [1]	34
3.2	Injection Current (amperes) versus electron concentration ($1/m^3$)	35
3.3	Injection Current (amperes) versus static photon concentration ($1/m^3$)	36
3.4	Transfer function of the laser which has been modeled as a filter	37
3.5	Variation of laser relaxation frequency with ε (m^3)	38
3.6	Variation of laser resonance frequency with ε (m^3)	39
3.7	Signal to intermodulation ratio (dB) versus modn. index for various values of ε	40
3.8	Signal to intermodulation ratio (dB) versus input frequency for various values of ε	41
3.9	Comparison of literature results	42
4.1	Fiber dispersion and chirp model	53
4.2	Variation of signal to intermodulation ratio (dB) with modn. index per channel	54
4.3	Variation of signal to intermodulation ratio (dB) with length of the fiber (m)	55
4.4	Variation of signal to intermodulation ratio (dB) with linewidth enhancing factor β_c	56
4.5	Variation of signal to intermodulation ratio (dB) with $\beta_2 L \beta_c$	57
4.6	Variation of signal to intermodulation ratio (dB) with $\beta_2 L \beta_c^2$	58
5.1	Simplified block diagram with sources of noise	69
5.2	FM Detector	70
5.3	AMPS SNR variation with received power for a) $N_0 = 10^{-10}$ and b) $N_0 = 10^{-12}$	71
5.4	TDMA BER variation with input power for a) $CNR_{background}$ = 10 dB and b) $CNR_{background}$ = 20 dB	72
6.1	Single signal dynamic range	80
6.2	Spur Free dynamic range	80
6.3	Effect of various nonlinearities versus modulation index	81
6.4	Combined nonlinearity versus input power (dBm)	82

6.5 AMPS SNR variation with input power for $N_0 = 10^{-10}$ 83
6.6 AMPS SNR variation with input power for $N_0 = 10^{-12}$ 84
6.7 BER for TDMA variation with input power (dBm) for $CNR_{background}$ = 10 dB 85
6.8 BER for TDMA variation with input power (dBm) for $CNR_{background}$ = 20 dB 86
6.9 Dynamic range (dB) versus number of active channels 87

LIST OF TABLES

Tables

3.1 Typical values of the physical parameters of lasers 33

Chapter1.

INTRODUCTION

Fiber optics has played a major role in the development of a variety of communication systems. It has been used extensively for transmitting digital signals over long distances. Recent experiments [1] have demonstrated the transmission of 2.5Gb/s data over distances as long as 4000 km. Also in the past 5 years, there has been a strong interest in the transmission of analog signals over fiber links. This has been motivated partly by the need to transmit cable television (CATV) signals over fiber. Recent research has led to a drastic improvement in the performance of fiber optic links used for analog transmission. Such systems have also been found to be useful in other communications applications, one of which is wireless communications [2,3]. The fiber is used as an interface between the wireless links. This thesis analyses some of the performance limitations of fiber optics systems used for wireless communications.

In this introduction, we first give a brief overview of wireless communications and fiber optics communications systems. We then discuss how fiber optics finds applications in wireless communications. We also give a brief overview of the work that has been done in this area. Finally, the research objectives and organization of this thesis are presented.

1.1 Review of Wireless Communications

Wireless communications has been one of the fastest growing industries in recent years. There has been a huge demand for better and more versatile wireless services. These systems use radio waves to provide a communications link between the transmitter and the receiver. Several standards have been used all over the world to provide communications within an allocated frequency band.

In the US, the TIA IS-19, known as the Advanced Mobile Phone System (AMPS), standard was proposed in the late 1970's. The entire region which is to be serviced is divided into smaller sections called cells. Each cell has a central basestation (central BS). The AMPS standard uses the frequency band of 824 MHz to 849 MHz for transmission from the mobiles to the central BS (uplink), and the frequency band of 869 MHz to 894 MHz for transmission from the central BS to the mobile (downlink). The frequency spectrum is divided into several channels (or Frequency Division Multiplexed FDM) and each channel (link between the mobile and the central BS) occupies 30 kHz frequency bandwidth. The speech is modulated using analog FM.

Recently a new digital standard, IS-54 has been used in several urban areas. It uses the same channel bandwidth of 30 kHz as AMPS, but now this channel is split between three users using Time Division Multiple Access (TDMA). A digital modulation technique called $\pi/4$ DQPSK is used in this standard. The information in the channel is split into frames. Each frame is divided into 6 time slots and each user accesses 2 slots per frame.

The third standard that is quickly gaining popularity uses the Code Division Multiple Access (CDMA) technique. In this scheme, the same frequency band is used by all the users, but now each channel is assigned a high bit rate pseudo noise (PN) sequence which is known only to the transmitter and the receiver. This PN sequence spreads the users narrow band information over a wide bandwidth that is shared by all the users. Only the receiver which knows the PN sequence can decode the information, while for the other receivers this information just appears as weak wideband interference.

As the demand for wireless services has increased, there have been several efforts to utilize the allocated frequency spectrum much more efficiently. One way to do this is to split each cell into smaller cells (called microcells). Each microcell has a micro base station (micro BS) which acts as the link between the mobiles in the micro cell and the central BS.

The radio frequency (RF) signals received at the micro BS can either be processed at the micro BS itself, or can be processed at the central BS. The need to make the micro BS as simple and cheap as possible makes the first approach inappropriate. The second scheme however means

that it is now necessary to provide signal communication between the micro BS and the central BS. Fiber links have been proposed for this purpose.

1.2 Fiber Optics Links used for Analog Transmission.

The simplest fiber optic link for radio signals is to allow the multi-frequency radio signal to directly intensity modulate the optical source. This scheme is called the Amplitude Modulated Subcarrier Multiplexed (AM-SCM) technique. To understand the concept of AM SCM, consider a multi channel signal such as the combined signal from several mobiles received at the central BS or a CATV signal. This signal is used to intensity modulate the laser diode. The intensity modulation process is shown in Fig. 1.1. In this process, the intensity of the optical signal that is emitted by the laser is varied by changing the modulation current of the laser. Then the optical signal that is emitted by the laser diode is an optical carrier that is intensity modulated by a signal that is composed of several individually modulated carriers. Each of these carriers are called subcarriers and the above technique is called AM SCM.

AM SCM techniques have been used to transmit CATV signals over optical fibers [4-7]. This technique is different from the usual digital transmission over the fiber. It requires much more stringent performance from the fiber optics link used because it is more susceptible to noise and distortion.

AM SCM has also been proposed [2] for communications between micro BS and the central BS. The architecture of such systems is described in the next section.

1.3 Architecture of Fiber Optics links for Wireless Communications Applications

The AM SCM technique described earlier is used for transmission of mobile signals (either AMPS or TDMA or both) between the micro BS and the central BS. There are several other alternatives to the AM-SCM technique. One of them is to digitize these signals at the micro BS and then send the digital signal over the fiber. The advantage of this technique is that considerably more noise and nonlinear distortion can be accommodated in the fiber link without degrading performance. However, the digitization of the signals has to be done at the micro BS. There is an imperative need that the micro BS be kept as small, simple and inexpensive as possible. The AM SCM technique is extremely simple and hence is the preferred technique.

The architecture of the AM SCM technique is shown in Fig. 1.2. The uplink signal received at the micro BS is the combination of signals from all the mobiles in the microcell. This signal is used to intensity modulate the laser diode. This AM SCM signal is then transmitted over fiber to the central BS. At the central BS, the signal is received by a photodetector and then the various channels are separated.

For the downlink mode, the central BS generates the signal that has to be sent to the mobiles in the microcell. This signal is then sent to the micro BS using AM SCM. It is detected at the micro BS using optical receivers.

As can be seen from fig 1.2, the micro BS has been kept extremely simple and the processing of the calls is done at the central BS.

Though this system looks extremely simple, it is not without its disadvantages. The main disadvantage is the excess noise and the nonlinear distortion that is introduced by the fiber optics system. There is also another problem which occurs with fiber optics systems used for wireless communications. The strength of the signal that is received at the micro BS changes with time. This is because as the mobiles get closer to the micro BS, the received strength increases. Similarly, as they move away from the micro BS, the received strength decreases. The total range over which the strength of the received signal can vary, without significant degradation due to noise and nonlinearity is called the dynamic range of the system. As will be seen, the allowed dynamic range depends on the noise and nonlinear distortion due to the fiber optics system.

In this thesis, we shall first study and model the various noise and nonlinearities introduced in the fiber link. We shall then study the effect of these impairments on the dynamic range for both AMPS and TDMA signals.

1.4 Previous Research

The use of the AM SCM technique for wireless communications was first proposed by Donald Fye in 1991 [2]. In this paper, Fye noted that the highly linear analog fiber optic links used for cable television systems were also ideally suited for use in cellular radio applications. He also

proposed an architecture and design of such a system. The major sources of noise and nonlinearity were recognized in this paper and the concept of dynamic range was explained.

Recognizing the impact the proposed system would have on communications, a considerable research was focused on understanding and improving the performance of fiber optic links for wireless communications. Shibutani, Kanai, Domom, Emura and Namiki [3] investigated the feasibility of the fiber optics link for microcellular systems using the GSM digital mobile telephone standard (GSM is the European digital cellular radio standard using TDMA technique) and also for an analog FDM standard like AMPS. The effect of increasing the number of channels received at the microcellular basestation on the nonlinear distortion and the dynamic range of the fiber links was also discussed. Morita and Ohtsuka [9] also described the features and benefits of the fiber optics link for wireless communications. They also proposed the use of a similar architecture in adaptive antenna arrays, terrestrial microwave radio and satellite communications. Winston Way [10] discussed the integration of these systems with the optical networks for fiber in the loop (FITL) applications (FITL is a project which brings the optical fiber into the subscriber loop distribution plant of the network) and also with cable television systems. He also proposed an alternate architecture based on external modulation of the laser [1] instead of the AM SCM system.

There has also been a lot of interest in techniques which enhance the dynamic range of the fiber optics system used in these applications. These techniques have been proposed and discussed extensively in [3,9-13].

Several ways of reduction in the nonlinearity have also been proposed in [14-17].

1.5 Organization of thesis.

Chapter 2 discusses the major sources of noise and nonlinearity in fiber optics systems used for analog applications. We shall also demonstrate which of these factors prove to be most significant in the microcellular mobile environment. Chapter 3 discusses the laser nonlinearity model which has been derived using the laser rate equations. Chapter 4 outlines the nonlinearity that is introduced because of the combination of laser chirp and fiber dispersion. In Chapter 5, we describe the major noise sources and also derive an analytical equation for the signal to noise ratio (SNR) for the AMPS signals. Chapter 6 combines the results from Chapter 3 to Chapter 5

to find the dynamic range for AMPS and TDMA signals. Conclusions are presented in Chapter 7.

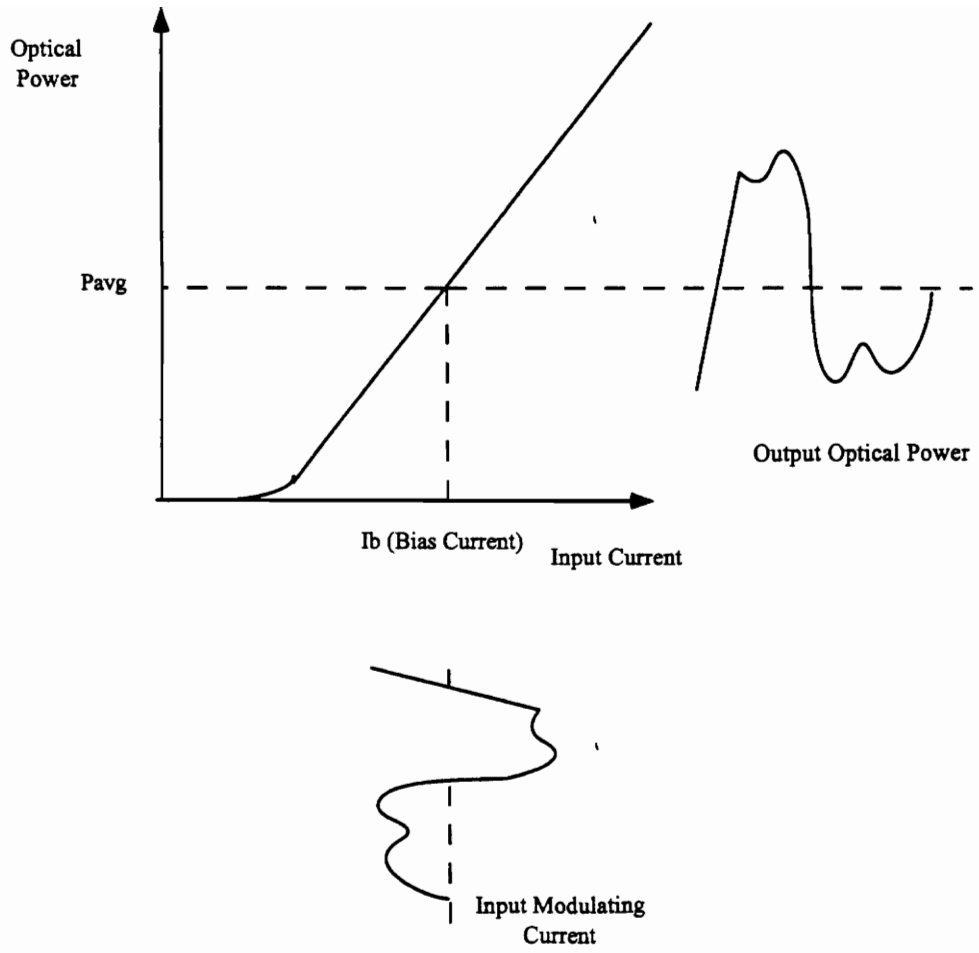

Figure 1.1 Intensity Modulation of Laser Diode

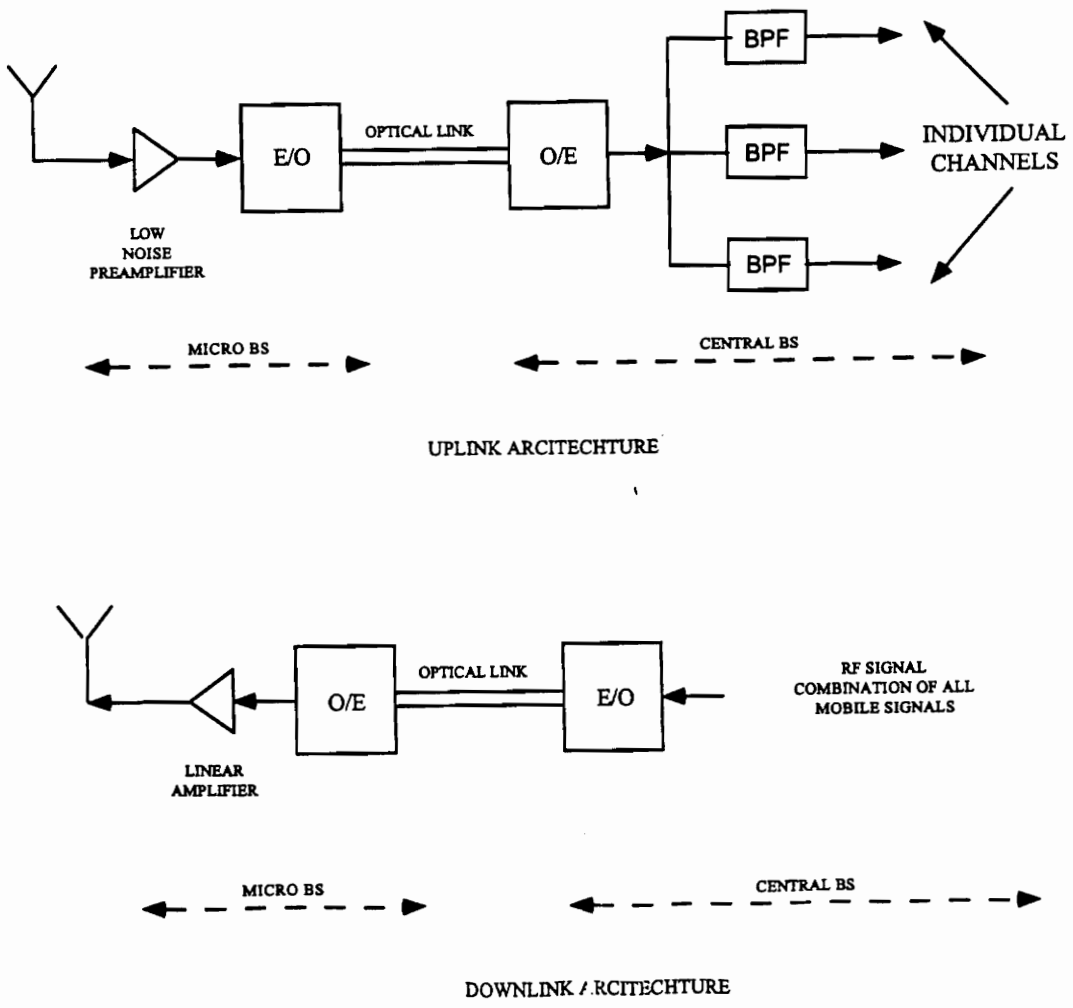

Figure 1.2 Architechture of the microcellular system using intensity modulated laser

Chapter 2.

NOISE AND NONLINEAR EFFECTS ON ANALOG TRANSMISSION

As seen in chapter 1, use of the AM SCM technique can simplify the design of the micro BS used in microcellular mobile radio systems. However, the fiber optics system introduces noise and nonlinear distortion in the mobile signal. In this chapter, we describe the major system impairments caused by the fiber link. We shall also investigate which of these are most significant and have to be considered further to determine their effect on the mobile signal.

2.1 Nonlinearities in the Fiber Optics Link

In AM-SCM systems, nonlinearity can be specified by the composite second order (CSO) and composite triple beat (CTB) intermodulation products resulting from the frequency beating of the carriers of the mobile signals. The CSO and CTB are the second order ($f_1 + f_2$) and third order ($f_1 + f_2 - f_3$) products which lie in the channel bandwidth of the mobile signals. In mobile communications the uplink frequency spectrum allocated for the AMPS signals is 824MHz to 849MHz. This means that the total width of the spectrum is 25MHz. As a result of the high carrier frequencies involved and the low width of the spectrum, all the second order products $f_1 + f_2$ and $f_1 - f_2$ fall outside the frequency band of 824MHz- 849MHz. As a result of this, in this analysis and further we do not consider the CSO nonlinearities. However the CTB nonlinearity products which lie at frequencies $f_1 + f_2 - f_3$ fall directly in the frequency band of the AMPS signals and are therefore the dominant distortion products in the fiber optics analog systems used for wireless radio applications.

CTB is measured relative to the carrier power of the fundamental signal and is specified in terms of dBc.

We shall now describe the factors which affect the nonlinear performance of such a system.

2.1.1 Gain Saturation in the Laser Diode

This type of nonlinearity results from the interaction of the electrons and the photons in the active region of the laser diode, which leads to a resonance phenomenon in lasers[1]. It is the major nonlinearity in laser diodes [1,18,19]. Gain saturation nonlinearity is dynamic in nature. It depends on the modulation frequency of the mobile signals. It is closely related to the resonance frequency of the laser diode. It increases sharply as the modulation frequency nears the resonance frequency.

Apart from the physical parameters of the laser diode, this nonlinearity depends on the frequency of the modulating signal, the input power at the laser diode and the number of active mobile channels.

As the modulation frequencies are close to the resonance frequency of the lasers (typically in the 1 - 10 GHz range), this is one of the significant nonlinearities. Modeling and evaluation of this nonlinearity is done in chapter 3.

2.1.2 Threshold Clipping

The nonlinear performance of AM-SCM systems is generally limited by the threshold clipping nonlinearity[22,23]. Consider the input current versus optical power curve of the laser shown in figure 2.1. As can be seen from this figure, the optical power emitted from the laser is zero until an input threshold current is reached. Beyond this current, the optical power rises nearly linearly with the current. In our application, the input current is a combination of signals from several mobile channels. If the number of channels is large, then this combined signal I(t), which modulates the laser, can be considered to be a gaussian random process. Then it is possible for I(t) to slip below the input threshold current at some time. Under these circumstances, the laser power is reduced to zero and

results in the clipping of the input signal. This clipping results in a nonlinear distortion which is referred to as threshold clipping. Threshold clipping was first identified as a fundamental limitation on the capacity of AM-SCM CATV systems by Saleh [22] in 1989.

Threshold clipping strongly depends on the modulation index per channel and the total number of active channels at the base station. The modulation index per channel is given by

$$m = \frac{\Delta I_{LD}}{I_B - I_{TH}} \tag{2.1}$$

where ΔI_{LD} is the peak modulation amplitude for the laser diode injection current caused by a single channel, I_B is the current at which the laser is biased and I_{TH} is the threshold current of the laser. In effect I_B - I_{TH} is the maximum input current swing possible without experiencing clipping.

As the total number of channels modulating the laser increases, then the rms modulation index of the combined optical signal is given by

$$\mu = \sqrt{\frac{Nm^2}{2}} \tag{2.2}$$

where N is the total number of channels at the laser diode. This parameter determines the threshold nonlinearity.

Now it has been shown [23] that threshold nonlinearity does not cause significant distortion until μ is about 30%. After this point it is the dominant nonlinearity and results in a very severe degradation in performance. In our system, with N = 56 (worst case possible, where one microbase station handles all the traffic of the entire cell and each of the voice channels is used), for the threshold nonlinearity to start setting in we would require a modulation index per channel of around 5.6%.

Fig. 2.2 [23] shows the experimentally measured curve of clipping induced third order intermodulation nonlinearity versus the rms modulation index μ. We can see that the

nonlinearity that is introduced because of clipping is constant for low values of μ (μ<0.3). This is because as discussed earlier for μ<0.3, clipping does not affect the performance of the system. The relatively weak nonlinearity at these low values of μ is because of gain saturation and the combination of dispersion and chirp. However as μ increases beyond 0.3, threshold clipping dominates over any other type of nonlinearity and we see a drastic degradation in the nonlinear performance. In this region, even a slight increase in the rms modulation index causes severe changes in the nonlinearity that is introduced. In a mobile environment, the signal that is received at the basestation is used to intensity modulate the laser. If the power in this received signal increases, in the absence of predistortion techniques, the modulation index also increases. As the received signal strength fluctuates randomly, the rms modulation index also changes randomly. Any increase in power, which causes the rms modulation index to rise above the clipping threshold, would cause a severe and unpredicatable degradation in the performance of the system. As a result it is important that the signal that modulates the laser never causes the modulation index to cross the clipping threshold limit.

2.1.3 Combination of Laser Chirp and Fiber Dispersion Nonlinearity

In the case of intensity modulated lasers, the output optical frequency changes when there is a change in the modulating current. This occurs because intensity changes cause a change in the carrier concentration in the active region, which in turn results in a change of index of refraction. This frequency variation is called "chirp". Chirp results in a larger linewidth of the laser than is given by the phase noise associated with the spontaneous emission. Linewidth of the laser is a measure of the range of wavelengths over which the laser emits the optical signal. This increased linewidth is characterized by the "linewidth enhancement parameter" of the laser. Chirp causes a phase modulation of the optical signal. In the absence of any other effects, this phase modulation of the optical signal doesn't cause any undesirable effect. This is because we are using direct intensity modulated optical signals. There is no information in the phase of the optical signal and a direct detection receiver is insensitive to the phase of the optical signal.

But now the fiber also introduces dispersion in the system. We normally use single mode fibers for AM SCM systems. In single mode fibers, the main source of dispersion is intramodal dispersion, which results from different optical wavelengths having different

group velocities in the fiber. Ordinary lasers do not emit light at a single wavelength, but rather emit it over a narrow spectral width. Intramodal dispersion depends on the spectral width of the laser and on the length of the fiber. It is described by the dispersion coefficient D which is the dispersion per unit transmission length per unit spectral width. It is usually specified in ps/(km-nm). In normal digital systems, dispersion leads to pulse broadening and limits the transmission bit rate.

Dispersion results in a nonlinear phase response (i.e. phase is a nonlinear function of frequency), as a consequence of which the phase modulation caused because of chirp gets converted into amplitude modulation. This results in nonlinear products at the intermodulation frequencies. It has been shown in [18,24] that this type of nonlinearity is one of the significant nonlinearities which must be considered in analog systems. It is modeled in chapter 4.

External modulation may be used to remove this source of nonlinearity [10]. In external modulation, the laser basically emits an unmodulated CW optical signal. This signal is then modulated using external modulators. The advantage of this scheme is that as the modulating current of the laser does not change, there is no chirp and consequently no nonlinearity. However external modulation schemes are expensive and have therefore not been widely used. Also, presently available external modulators have fairly high insertion loss (typically greater than 3 dB) which reduces the already limited power budget of AM-SCM systems.

2.1.4 Fiber Nonlinearity

The major nonlinearities introduced because of the fiber are [1]:

Stimulated Raman Scattering(SRS):
Raman scattering results from the inelastic scattering of the photons due to molecular vibrations inside the silica fiber. The critical power level for Raman scattering to degrade the system performance is [25]

$$\frac{g_R L_e P}{bA_e} \approx 16 \qquad (2.3)$$

where g_R is the Raman gain, L_e is the effective length of the fiber, which is slightly shorter than the actual length of the fiber to account for the attenuation, P is the input power, b is a parameter which depends on the polarization properties of the fiber (b = 1 for polarization preserving fibers and b = 2 for normal fibers which do not preserve polarization) and A_e is the effective core area of the fiber.

For $g_R = 7(10)^{-12}$ cm/W, L_e = 5km, b = 2, $A_e \approx A = 5(10)^{-7}$ cm^2 , then P ≈ 1W, which is much greater than the powers used for normal fiber optics systems. Hence we can conclude that SRS is not major factor in the subcarrier multiplexed systems used for mobile communications.

Self Phase Modulation:

The refractive index of the fiber is not constant, but varies with the intensity of signal as [1]

$$n = n_0 + n_2 I \tag{2.4}$$

where n_0 is the ordinary refractive index associated with the material, n_2 is the intensity dependent refractive index, and I is the optical intensity. This effect is called the Kerr effect. It is a significant factor in very long digital systems using optical amplifiers as intermediate repeaters.

Consequently, the phase of the light after propagating through the fiber with length L (relative to the phase of the injected light) is

$$\Phi(L) = \frac{2\pi n_0 L}{\lambda} + \frac{2\pi n_2 I L}{\lambda} \tag{2.5}$$

A typical value of n_2 is $3(10)^{-16}$ cm^2/W. This weak dependence of the refractive index on the power, combined with the fact that we are not going long distances over the fiber (≈ 5 km) make this effect a minor contributing factor in the input signal degradation.

Stimulated Brillouin Scattering (SBS):

SBS is similar to SRS except that the SBS gain coefficient in single-mode fibers is over two orders of magnitude larger ($g_B \approx 4(10)^{-9}$ cm/W) than the SRS gain coefficient. Also the optical bandwidth for SBS is around 20MHz at 1.55μm. Thus maximum SBS gain will occur for lasers with linewidths less than 20MHz.

The critical power level at which SBS degrades the system performance is [25]

$$P_c = \frac{21bA_e}{g_B L_e} \tag{2.6}$$

where P_C is the input power and the other parameters are the same as in Raman scattering. For the typical parameters used above, $P_C \approx 4$mW. Thus we see that SBS is the dominant fiber nonlinearity which can affect the signal performance.

It has been experimentally observed that SBS degrades the CNR performance especially after the power level exceeds the Brillouin threshold power [26].

Figure 2.3 shows the variation of Brillouin threshold with the linewidth enhancing factor of the laser. The linewidth enhancing factor is a measure of the spectral linewidth of a laser and varies as the square root of the spectral linewidth of the laser. This variation has been obtained by assuming $g_B = 4(10)$-9 cm/W at 1.55μm and for a linewidth enhancing factor of 5. Since g_B is inversely proportional to the square of the laser linewidth factor, the Brillouin threshold power increases for increasing linewidth enhancing parameters. We can see that even for very small linewidth enhancing factors, the Brillouin threshold is larger than the input powers normally used for AM-SCM applications. Typical linewidth enhancing parameters for semiconductor lasers are in the range 5 to 6. As a result of this, in this study we shall not model Brillouin scattering nonlinearity.

From the above discussion, we see that gain saturation and dispersion and chirp nonlinearity have to be considered at all input powers and modulation indices. Threshold nonlinearity can be controlled by keeping the modulation index below the clipping limit.

2.2 Noise in Fiber Optics system

There are three main sources of noise in analog fiber optics systems: 1) Thermal noise of the receiver, 2) Shot noise of the photodetector and 3) Relative Intensity Noise (RIN) of the laser diode. Thermal noise results because of the thermal excitation of the electrons inside the photodetector load resistance. Shot noise arises from the statistical nature of the production and collection of the photoelectrons when optical light is incident on a photodetector. RIN is the fluctuation in the intensity of a semiconductor laser diode even when the laser is biased at a constant current with negligible current fluctuations. This is attributed to the spontaneous emission of photons inside the laser. These emissions add random amplitude and phase fluctuations to stimulated emission. The noise that results because of this effect is called relative intensity noise (RIN) of the laser. This noise has a bandwidth related to the relaxation frequecy of the laser. The spectral density of this noise, relative to the signal intensity is denoted in the equations by rin. It is represented in dB/Hz. Lasers typically have a rin of about -120 dB/Hz. Thus, for a 1 GHz bandwidth, the RIN is 30 dB below the signal level, which is negligible for a digital system, but is highly important in analog systems requiring high SNR. Lasers designed for analog applications now have rin as low as -160 dB/Hz [1].

The Carrier to Noise Ratio (CNR) per channel is given by [1]

$$CNR = \frac{\frac{1}{2} m^2 \Re^2 P_0^{\,2}}{rin\, \Re^2 P_0^{\,2} B + 2q\Re P_0 B + < i_{th} >^2 B} \qquad (2.7)$$

where $\Re$ is the responsivity of the photodetector, P_0 is the average received power, B is the bandwidth of the signal, $<i_{th}>^2$ is the thermal noise spectral density and q is the electron charge. In this equation the first term in the denominator results from the RIN of the laser, the second term results from the shot noise and the third term results from the thermal noise.

Figure 2.4 shows a plot of CNR against the average received power P_0. In this plot, we have used $\Re$ = 0.93 mA/mW [23], modulation index, m = 3%, $\sqrt{<i_{th}^2>}$ = 7 pA/$\sqrt{Hz}$, rin = -150 dB/ Hz and B = 30 KHz. We can easily see the various regions where each of the noise introducing factors is dominant. However the maximum CNR that is obtained is

limited by RIN of the laser. Hence RIN is an extremely important parameter in the analog transmission links using Fiber Optics. Presently lasers are being developed for analog applications having RIN as low as -160 dB/ Hz.

2.3 Summary

In this chapter we presented a review of the system impairments in the fiber optics links used for analog applications. Nonlinear distortion gives rise to intermodulation products. Second order intermodulation falls outside the band of interest in mobile systems and the dominant effects are given by the third order intermodulation. The principal causes of nonlinearity are gain saturation and the interaction between dispersion and chirp nonlinearity. However beyond a modulation index threshold, clipping sets in as the most dominant nonlinearity. In chapter 3 and chapter 4, we model and evaluate the effects of gain saturation and dispersion. In chapter 5, we also review the noise impairments of such systems and use this information to find the signal to noise ratio in the AMPS signal and the approximate bite error rate for TDMA signals. In chapter 6, we will show how noise and nonlinearity affect the dynamic range of the system.

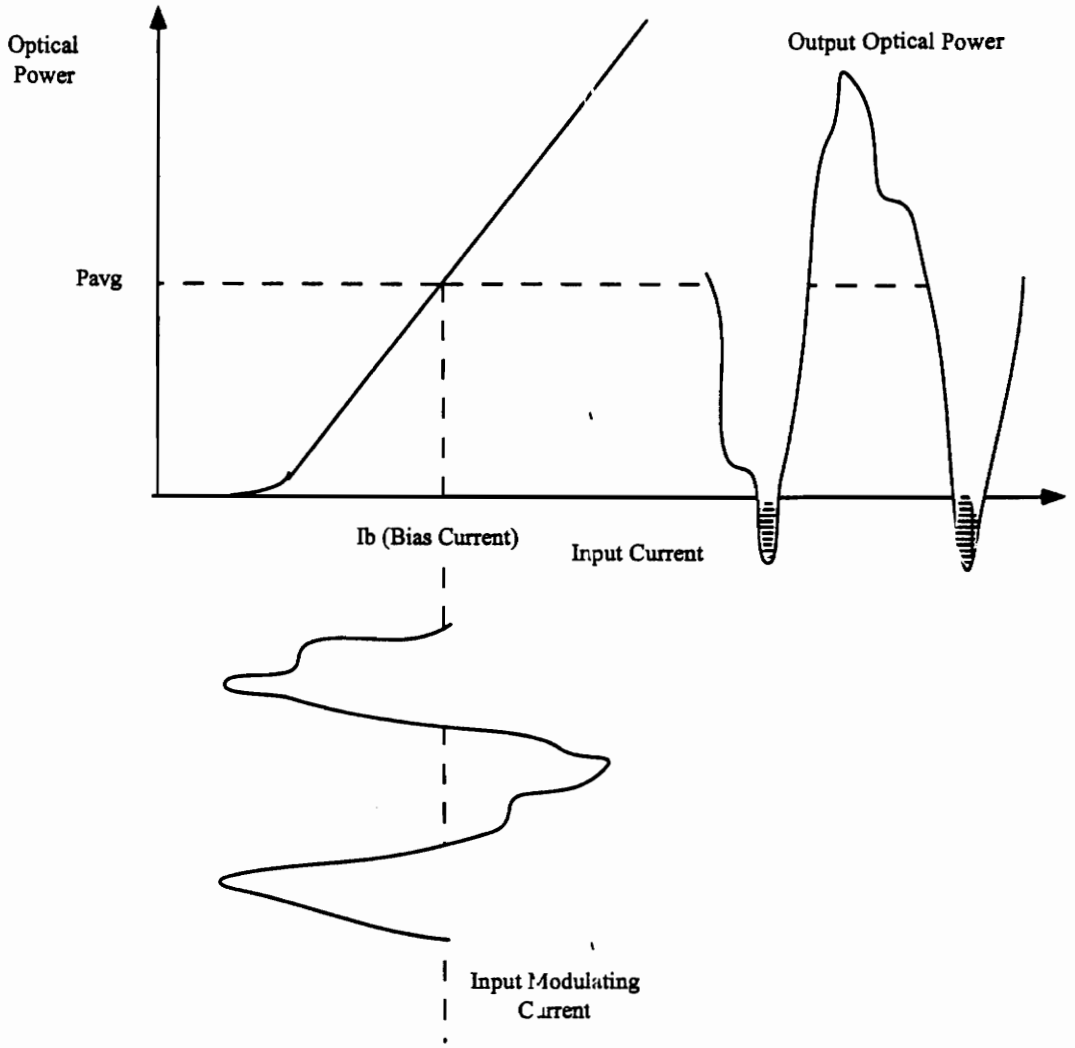

Figure 2.1 Threshold Clipping of Laser

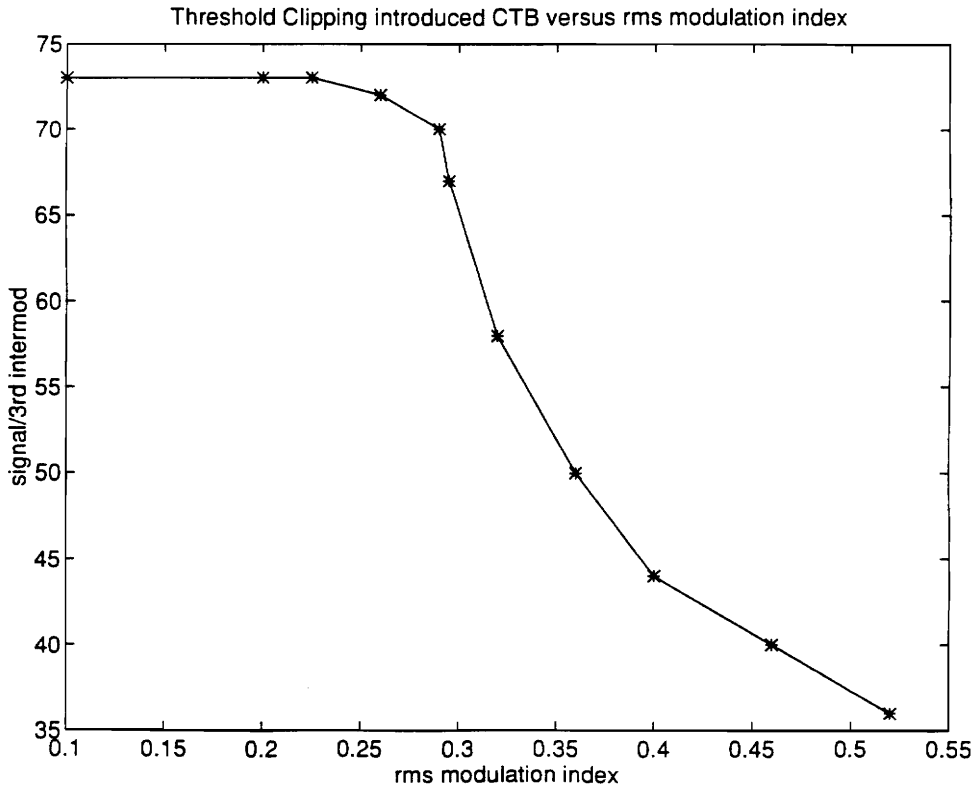

Figure 2.2 Third Order nonlinear distortion versus rms modulation index μ [23]

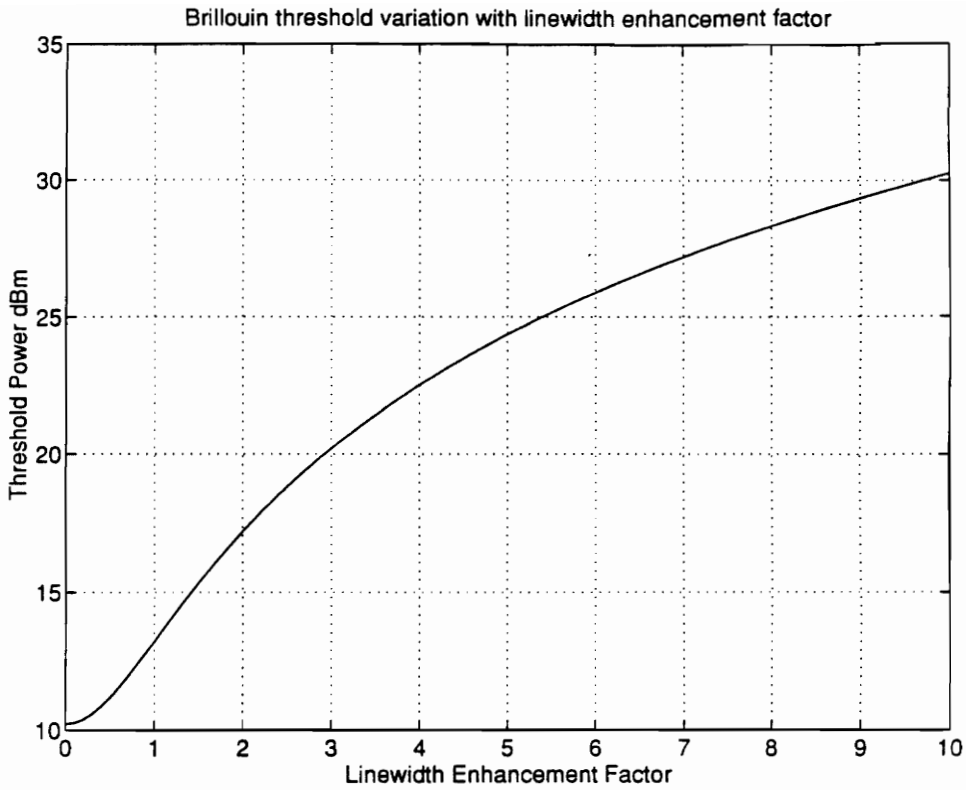

Figure 2.3 Variation of the input threshold power at which SBS degrades the noise performance versus the linewidth enhancing factor of the laser

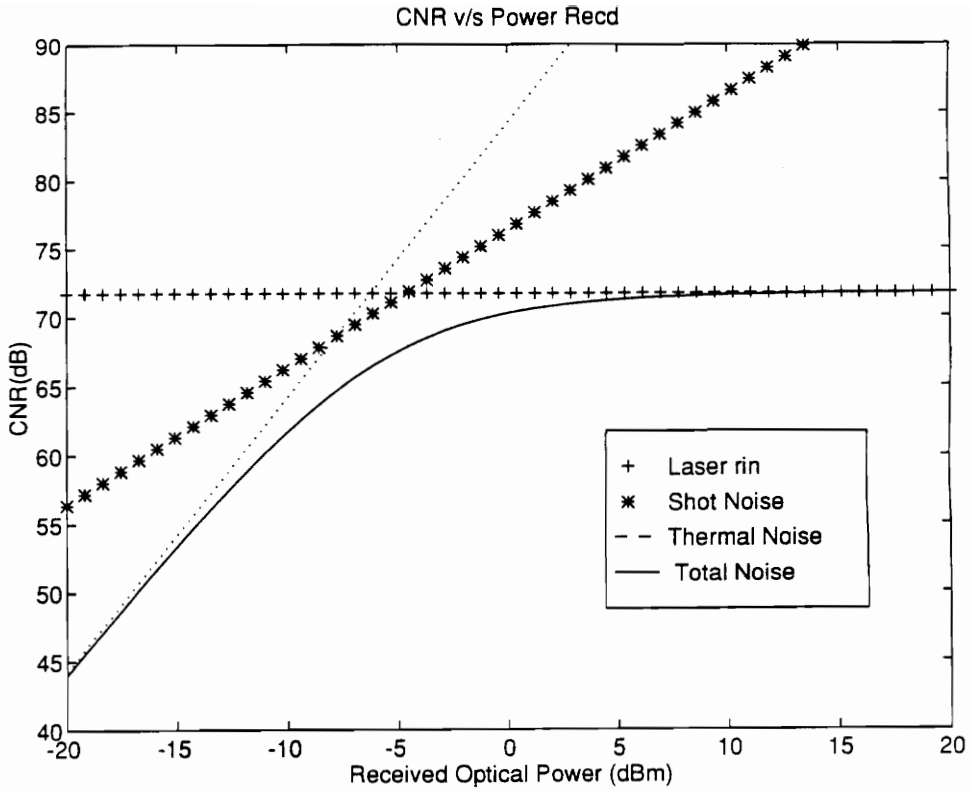

Figure 2.4 CNR versus average received power P0, showing regions where the receiver thermal noise, shot noise and the laser RIN noise are dominant

Chapter 3.

GAIN SATURATION IN LASER DIODES

In chapter 2, we discussed the factors which introduce nonlinear distortion in analog signals, when they are sent over fiber links using AM-SCM modulation. We saw that one of the factors which required further modeling was gain saturation in the laser. This nonlinearity is closely related to the resonance phenomenon in lasers [1]. The nature of this nonlinearity is dynamic, i.e. it depends on the frequency of the modulating signal and is not memory free.

In this chapter, we shall model gain saturation using the laser rate equations. We shall also investigate dependence of this nonlinearity on factors such as modulation index, modulating frequency and the physical parameters of the laser.

3.1 Overview of Gain Saturation

Lasers generate light by stimulated emission of photons. This is in contrast to LED's which generate light by spontaneous emission. For stimulated emission to occur, it is necessary that population inversion take place. Population inversion between two energy states occurs when there are more electrons in the higher state than in the lower state. This cannot occur naturally, but can occur by appropriate excitation (pumping). In semiconductor lasers this excitation is provided by a bias current which injects minority carriers across the PN junction. Population inversion is reached when the density of the injected electrons in the active region exceeds a certain value called the transparency value (N_T). After this stage, the active region exhibits optical gain. The optical gain is proportional to the difference between the rate of stimulated emission R_{stim} and the rate of absorption R_{abs}. Figure 3.1 [1] shows the optical gain for a typical laser diode.

When the electron concentration (N) is less than N_T, the gain is negative (the material is absorbing) as there is no population inversion, as a result of which there is no stimulated emission. As N becomes greater than N_T population inversion occurs and gain becomes positive. Larger N results in a stronger population inversion and results in a higher optical gain.

It can be seen from this Fig.ure that as the photon concentration increases beyond a certain value, the gain starts dropping. This is called gain saturation. The physical reason for this is that as the stimulated emission increases, population inversion decreases resulting in reduction of optical gain.

Gain saturation nonlinearity is closely associated with the phenomena of spectral hole burning and spatial hole burning. Spectral hole burning causes a sharp decrease in the gain at some wavelengths. It can be attributed to the fact that some wavelengths experience selective gain saturation. As a result of this the gain at these wavelengths drops sharply causing a spectral hole in the gain at these wavelengths. Spatial hole burning is another phenomenon that is not as strong as spectral hole burning [18]. It causes sharp dips in the gain at some points along the length of the active region of the length of the laser. In distributed feedback (DFB) lasers it is due to the nonuniform reflectivity that is induced by the DFB grating of the laser. This nonuniform reflectivity causes a nonuniform distribution of the optical intensity along the length of the laser as well as a nonuniform carrier concentration. As a result, at some points along the length of the laser, higher optical intensity causes gain saturation. This results in a decrease of the gain at these points.

3.2 Laser Rate Equations

The characteristics of semiconductor lasers can be well described by a set of nonlinear differential equations called the laser rate equations. These equations govern the interactions of the photons and the electrons in the active region of the laser. The laser rate equations can be derived from the Maxwell's Equations together with a quantum-mechanical approach for the induced polarization [1]. However, they can also be phenomenologically derived by considering the various phenomena occurring inside the laser which result in the creation and destruction of photons and electrons. The laser rate equations are:

$$\frac{dN}{dt} = -\gamma(N - N_T)S + \frac{I\Gamma_e}{qV} - \frac{N}{\tau_c} \tag{3.1}$$

$$\frac{dS}{dt} = \Gamma\gamma(N - N_T)S - \frac{S}{\tau_p} + \frac{\Gamma\beta N}{\tau_c} \tag{3.2}$$

where N is the electron density in the active region, γ is the differential gain, N_T is the transparency electron concentration, S is the photon density in the active region, I is the injection current, Γ_e is the electron confinement factor, τ_c and τ_p are the spontaneous carrier lifetime and the photon lifetime respectively, Γ is the optical confinement factor, β is the fraction of the spontaneous emission that is coupled into the active region, and q is the electron charge.

The rate equations can be interpreted as follows. The three terms on the right hand side of eqn 3.1 signify the rates at which electrons are created or lost in the active region of the laser. The first term gives the loss of electrons by electron-hole recombination through stimulated emission. The second term is the gain of the electron due to the injection current. The third term is the loss of electrons by spontaneous emission.

We can similarly explain eqn. 3.2. In this equation, the first term on the right hand side signifies the rate of creation of the photons due to stimulated emission. The second term is the depletion of the photons due to cavity losses. The third term is the creation of photons due to spontaneous emission.

To account for nonlinearity, the rate equations can be modified by including a gain saturation parameter ε. In the rate equations the differential gain γ is replaced by $\gamma = \gamma/(1 + \varepsilon S)$. If $\varepsilon S << 1$, then $\gamma/(1 + \varepsilon S) \approx \gamma(1 - \varepsilon S)$. ε is dependent on the spectral hole burning. The modified equations are [27]

$$\frac{dN}{dt} = -\gamma(N - N_T)(1 - \varepsilon S)S + \frac{I\Gamma_e}{qV} - \frac{N}{\tau_c} \tag{3.3}$$

$$\frac{dS}{dt} = \Gamma\gamma(N - N_T)(1 - \varepsilon S)S - \frac{S}{\tau_p} + \frac{\Gamma\beta N}{\tau_c} \tag{3.4}$$

We use this equation for further analysis.

3.3 Nonlinear Modeling

If we do the analysis for small signal modulation, then we can write

$$I = \bar{I} + i(t) \tag{3.5}$$

$$S = \bar{S} + s(t) \tag{3.6}$$

$$N = \bar{N} + n(t) \tag{3.7}$$

where $\bar{I}, \bar{S}$ and $\bar{N}$ are the average (bias) values of the current, photon density and electron density respectively and i(t), s(t) and n(t) are the time varying injection current, photon concentration and electron concentrations respectively.

The steady state solution occurs when $\frac{dN}{dt} = 0, \frac{dS}{dt} = 0, N \neq 0, S \neq 0.$

Then from 3.3 and 3.4 we obtain the following expression for $\bar{N}$ and $\bar{S}$ in terms of laser parameters

$$\bar{N} = \frac{\frac{\bar{S}}{\tau_p} + N_T \Gamma \gamma (1 - \varepsilon \bar{S}) \bar{S}}{\frac{\Gamma \beta}{\tau_c} + \Gamma \gamma (1 - \varepsilon \bar{S}) \bar{S}} \tag{3.8}$$

$$\frac{\bar{N}}{\tau_c} + \gamma (\bar{N} - N_T)(1 - \varepsilon \bar{S}) \bar{S} = \frac{\bar{I} \Gamma_e}{qV} \tag{3.9}$$

The above equations are solved numerically to give the steady state values of the electron and the photon concentrations. Figures 3.2 and 3.3 show the variation of the photon and electron concentrations with the injection current. In these plots, we have taken typical values of the parameters in the table 3.1.

Figures 3.2 and 3.3 give the static characteristics of the laser caused resulting from gain saturation. The photon concentration has been plotted in Fig. 3.3 as a function of injection current for two different values of the gain saturation parameter ε. We see that the effect of gain saturation on the photon concentration (and hence on the optical power emitted) is to cause a reduction in the photon concentration for increasing values of ε. Although increasing ε reduces the slope of the photon concentration v/s the injection current curve, this curve remains linear. Therefore the rate equation analysis does not give a static nonlinearity in the laser characteristics above the threshold. However, as will be shown below, there is a dynamic nonlinearity. Also, the threshold behaviour is clearly indicated in Fig. 3.3. Thus threshold clipping for signals which fall below the threshold current can be evaluated using the steady state analysis. Evaluation of the effect of gain saturation requires considering dynamic effects.

We consider the case when the input current modulating the laser is a combination of three input sinusoids at frequencies ω_1, ω_2 and ω_3 respectively. Then we have

$$i(t)=i_{11}(t)e^{j\omega_1 t}+i_{12}(t)e^{j\omega_2(t)}+i_{13}(t)e^{j\omega_3 t} \qquad (3.10)$$

where i_{11}, i_{12} and i_{13} are the amplitudes of the injection current at frequencies ω_1, ω_2 and ω_3 respectively.

Modulating the laser with an input signal which is the combination of three sinusoids results in modulation of the electron and photon concentrations inside the laser. The photon and electron concentrations are modulated not only at the fundamental frequencies but also there are components at the harmonic and intermodulation frequencies. In this analysis, we consider only the third order intermodulation frequencies. So we can write the photon and electron concentrations as

$$\begin{aligned} s(t)= \; & s_{11}(t)e^{j\omega_1 t}+s_{12}(t)e^{j\omega_2 t}+s_{13}(t)e^{j\omega_3 t}\,(\text{Fundamental terms})+ \\ & s_{31+1-2}(t)e^{j(2\omega_1-\omega_2)t}+s_{31+1-3}(t)e^{j(2\omega_1-\omega_3)t}+s_{32+2-1}(t)e^{j(2\omega_2-\omega_1)t}+ \\ & s_{32+2-3}(t)e^{j(2\omega_2-\omega_3)t}+s_{33+3-1}(t)e^{j(2\omega_3-\omega_1)t}+s_{33+3-2}(t)e^{j(2\omega_3-\omega_2)t}+ \end{aligned}$$

$$s_{31+2-3}(t)e^{j(\omega_1+\omega_2-\omega_3)t} + s_{31-2+3}(t)e^{j(\omega_1-\omega_2+\omega_3)t} + + s_{32+3-1}(t)e^{j(\omega_2+\omega_3-\omega_1)t}$$
$$+ \text{other nonlinear terms (second order and other higher order terms)} \qquad (3.11)$$

where s_{11}, s_{12} and s_{13} are the amplitudes of the photon concentrations at the fundamental frequencies ω_1, ω_2 and ω_3 respectively. Also s_{31+1-2} is the amplitude of the component at $2\omega_1-\omega_2$ and s_{31+2-3} is the amplitude of the component at $\omega_1+\omega_2-\omega_3$.

Similarly, we can write the electron concentration as

$$\begin{aligned} n(t) = {} & n_{11}(t)e^{j\omega_1 t} + n_{12}(t)e^{j\omega_2 t} + n_{13}(t)e^{j\omega_3 t}\,(\text{Fundamental terms}) + \\ & n_{31+1-2}(t)e^{j(2\omega_1-\omega_2)t} + n_{31+1-3}(t)e^{j(2\omega_1-\omega_3)t} + n_{32+2-1}(t)e^{j(2\omega_2-\omega_1)t} + \\ & n_{32+2-3}(t)e^{j(2\omega_2-\omega_3)t} + n_{33+3-1}(t)e^{j(2\omega_3-\omega_1)t} + n_{33+3-2}(t)e^{j(2\omega_3-\omega_2)t} + \\ & n_{31+2-3}(t)e^{j(\omega_1+\omega_2-\omega_3)t} + n_{31-2+3}(t)e^{j(\omega_1-\omega_2+\omega_3)t} + + n_{32+3-1}(t)e^{j(\omega_2+\omega_3-\omega_1)t} \\ & + \text{other nonlinear terms (second order and other higher order terms)} \qquad (3.12) \end{aligned}$$

Now we use equations 3.10, 3.11, and 3.12 to solve the rate equations 3.3 and 3.4. We differentiate the eqns 3.10, 3.11 and 3.12 and then equate the equal frequency terms. Let us first do this for one of the fundamental frequencies ω_1. At this frequency we get

$$j\omega_1 n_{11} = \frac{i_{11}\Gamma_e}{qV} - An_{11} - Bs_{11} \qquad (3.13)$$

$$j\omega_1 s_{11} = Cn_{11} + Ds_{11} \qquad (3.14)$$

where

$$A = \frac{1}{\tau_c} + \gamma\bar{S}(1-\varepsilon\bar{S})$$

$$B = \gamma(\bar{N}-N_T)(1-\varepsilon\bar{S}) - \gamma(\bar{N}-N_T)\varepsilon\bar{S}$$

$$C = \frac{\Gamma\beta}{\tau_c} + \Gamma\gamma\bar{S}(1-\varepsilon\bar{S})$$

$$D=\Gamma\gamma(\bar{N}-N_T)(1-\varepsilon\bar{S})-\Gamma\gamma(\bar{N}-N_T)\varepsilon\bar{S}-\frac{1}{\tau_p}$$

And at the intermodulation frequency, we can write

$$j(2\omega_1-\omega_2)n_{31+1-2}=-An_{31+1-2}-Bs_{31+1-2}-E(s_{11}{}^2n_{12}) \quad (3.15)$$

$$j(2\omega_1-\omega_2)s_{31+1-2}=Cn_{31+1-2}+Ds_{31+1-2}+F(s_{11}{}^2n_{12}) \quad (3.16)$$

Similarly at frequency ($\omega_1 + \omega_2$ - ω_3) we obtain

$$j(\omega_1+\omega_2-\omega_3)n_{31+2-3}=-An_{31+2-3}-Bs_{31+2-3}-E(s_{11}s_{12}n_{13}) \quad (3.17)$$

$$j(\omega_1+\omega_2-\omega_3)s_{31+2-3}=Cn_{31+2-3}+Ds_{31+2-3}+F(s_{11}s_{12}n_{13}) \quad (3.18)$$

where

$$E = -\gamma\varepsilon \quad (3.19)$$

$$F = \Gamma\gamma\varepsilon \quad (3.20)$$

Then solving eqn's 3.13 and 3.14, we get

$$s_{11}=\frac{\frac{Ci_{11}\Gamma_e}{qV}}{((j\omega_1+A)(j\omega_1-D)+BC)} \quad (3.21)$$

Equation 3.21 gives the relation between the photon concentration at the fundamental frequency, the input current and the frequency of the modulating current. The photon concentration and the optical power are related as

$$P=\frac{s}{x},$$

where $x=\frac{2\Gamma\tau_p\Gamma_e}{V\eta h\upsilon}$,

and where P is the optical power, s is the photon concentration, υ is the frequency, η is the quantum efficiency and h is the Planck's constant. In this equation, $\frac{sV}{\tau_p}$ is the number of photons lost per second by the cavity, $h\upsilon$ is the energy per photon, $\frac{\eta}{\Gamma\Gamma_e}$ is the fraction of

photon loss that is external and we assume that only half of the photons that are lost are emitted from the face coupled to the fiber.

Using the above relationships, we can plot the transfer function of the laser. This is shown in Fig.ure 3.4. Again the typical parameters from the table 3.1 have been used. The response is flat at low frequencies, exhibits a resonance, and then falls off.

From eqn 3.1.21, we can express the transfer function of the laser as

$$|H(\omega)|^2 = \left| \frac{\frac{s(\omega)}{i(\omega)}}{\frac{s(0)}{i(0)}} \right|^2 = \frac{(BC - AD)^2}{(BC - AD - \omega^2)^2 + \omega^2 (A - D)^2} \tag{3.22}$$

The transfer function of the laser may be expressed as [27]

$$|H(\omega)|^2 = \frac{{\Omega_R}^4}{({\Omega_R}^2 - \omega^2)^2 + {\Gamma_R}^2 \omega^2} \tag{3.23}$$

where Ω_R is the relaxation frequency and Γ_R is the damping frequency. Comparing 3.1.22 and 3.1.23, we can write the relaxation frequency as $\sqrt{BC - AD}$ and the damping frequency is given by (A-D). Also in eqn. 3.1.23, the resonance frequency Ω_0(where $H(\omega)$ is maximum) of the laser is given by

$$\Omega_0^2 = \Omega_R^2 - \Gamma_R^2/2 \tag{3.24}$$

Then the resonance frequency in terms of the parameters A, B, C and D is given by

$$\Omega_0 = \sqrt{BC - \frac{A^2 + D^2}{2}} \tag{3.25}$$

In Fig. 3.5, we show the variation of the relaxation frequency with the gain saturation parameter ε. We see from Fig. 3.5 a very weak dependence on the gain saturation parameter. The relaxation frequency depends on the physical parameters of the laser and the average photon concentration inside the active region of the laser. In Fig. 3.6, the variation

of the resonance frequency versus the gain saturation parameter is shown. The resonance frequency is much more dependent on the gain saturation parameter.

Also solving 3.15 and 3.16, we obtain

$$s_{31+1-2} = \frac{F(n_{11}s_{11}s_{12})(j(2\omega_1 - \omega_2) + A) - E(n_{11}s_{11}s_{12})}{\left(\frac{(j(2\omega_1 - \omega_2) + A)(j(2\omega_1 - \omega_2) - D)}{C} + B\right)} \tag{3.26}$$

Similarly, solving equations 3.17 and 3.18, we get the photon concentration at the intermodulation frequency ($\omega_1+\omega_2-\omega_3$) as

$$s_{31+2-3} = \frac{F(n_{11}s_{12}s_{13} + s_{11}n_{12}s_{13})(j(\omega_1 + \omega_2 - \omega_3) + A) - E(n_{11}s_{12}s_{13} + s_{11}n_{12}s_{13})}{\left(\frac{(j(\omega_1 + \omega_2 - \omega_3) + A)(j(\omega_1 + \omega_2 - \omega_3) - D)}{C} + B\right)} \tag{3.27}$$

The third order nonlinear distortion to carrier ratio is given as

$$3IMD = \left(\frac{s_{3x+y-z}}{s_{1a}}\right)^2 \tag{3.28}$$

where s_{3x+y-z} is the third order photon concentration at the frequency x+y-z, and s_{1a} is the photon concentration at the fundamental frequency a.

As can be seen from equations 3.19,3.20, 3.27 and 3.28 if $\varepsilon = 0$, $E = F = 0$ and hence both s_{31+1-2} and s_{31+2-3} become 0. This implies that with no gain saturation, the dynamic nonlinearity reduces to 0. Also as is obvious from further discussion, but which can also be understood from these equations is that as ε increases, the nonlinearity increases.

We use the above developed equations to determine and investigate deeper into the gain saturation nonlinearity.

3.4 Variation of the nonlinearity with various physical parameters.

In this section, we discuss the behavior of the laser model when it is subjected to changes in the important physical parameters of the laser and also the variations in the input modulating current. Table 3.1 summarizes the various parameters which we have used so far and also provides typical numerical values which have been used.

Figure 3.7 shows the variation of the nonlinearity with the modulation index for various values of the gain saturation parameter. The linearity of the laser increases with decreases in ε. As was shown analytically in the earlier section, the nonlinearity reduces to 0 at $\varepsilon = 0$. The gain saturation parameter is extremely important and a slight perturbation in this value causes significant change in the nonlinearity. Also from this analysis we note that the nonlinearity increases as the modulation index is increased. The signal to intermodulation ratio decreases by 40 dB for every decade increase in the modulation index. Therefore, the signal to intermodulation ratio is inversely proportional to m^4. This is a consequence of the fact that signal strength is proportional to m^2, whereas the strength of the third order intermodulation product is proportional to m^6.

A modulation index per channel between 0.04 and 0.05 is typically used in AM SCM systems. Also in this analysis, we have not considered the effect of threshold clipping. As was discussed earlier, the effect of threshold clipping sets in as m approaches 0.06 when the number of channels gets near 56.

Figure 3.8 shows the effect of modulation frequency on the nonlinearity. In this plot, the three modulation frequencies f_1, f_2 and f_3 are such that f_1+1MHz = f_2 and f_2+1MHz = f_3. We investigate the nonlinearity at the lowest frequency channel, f_1. We observe that the nonlinearity is fairly independent of the frequency for low modulation frequencies. But as the modulation frequency gets near the resonance frequency of the laser, the nonlinearity increases sharply. Normal resonance frequencies of the lasers are around few GHz. The modulation frequency of the mobile signals are between 800MHz and 900MHz. As a result the effect of change in the modulation frequency affects the nonlinear performance of the fiber link. This is also the reason why it may not be appropriate to use a simple memory free

static nonlinearity (as can be modeled by a power curve of the type $P(t) = a_1 i(t) + a_2 i(t)^2 + a_3 i(t)^3$) for such an analysis.

In Fig. 3.9, we compare the gain saturation model that was developed in this chapter with the analytical or experimental results that have been quoted in the literature [3,19,30]. We see that there is a lot of variability in the quoted results. This is because the models for nonlinearity are very susceptible to the parameters that have been used and the approximations made during the analysis. Very slight differences in these factors cause changes in the final results. But we can notice from Fig. 3.9, that the behavior of this nonlinearity with the optical modulation index is similar, i.e. the nonlinearity varies directly with m^2. Also the decrease in the signal to the intermodulation ratio with increase in the modulating frequency has been noted in [18]. We also note that the results obtained in this analysis are optimistic compared to those obtained in the literature. This may be because we have not considered static nonlinearity caused because of temperature changes and other factors.

3.5 Summary

In this chapter, we described the development of the laser model for treating gain saturation. We also discussed the effect of modulation index, modulation frequency and the gain saturation on the nonlinearity. It was observed that for the frequency range of the mobile signals, it is appropriate to make use of this model instead of a static nonlinearity model. In the next chapters, we shall combine the results obtained from this chapter to the dispersion and chirp model and use them to find the total nonlinear distortion due to the fiber link.

Table 3.1 Typical values of the physical parameters for lasers

Symbol	Definition	Typical Value	Unit
N, n	electron density		m^{-3}
S, s	photon density		m^{-3}
I, i	injection current		amperes
q	electron charge	$1.6(10)^{-19}$	Coulombs
γ	differential gain	$2(10)^{-12}$	m^3/s
N_T	transparency electron density	$1.2(10)^{24}$	m^{-3}
ε	gain saturation factor	$3(10)^{-23}$	m^3
τ_p	photon lifetime	$1.4(10)^{-12}$	sec
τ_c	carrier lifetime	$3(10)^{-9}$	sec
Γ	optical confinement factor	1	
Γe	electron confinement factor	0.7	
V	volume	$1.8(10)^{-18}$	m^3

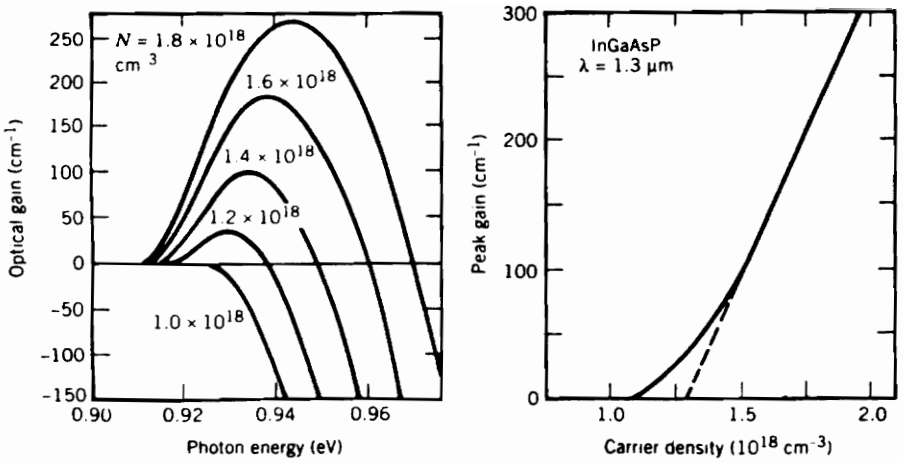

Calculated gain coefficient and its frequency dependence for a 1.3-μm InGaAsP active layer for several values of the injected carrier density N. (*a*) Gain g as a function of the photon energy; (*b*) variation of peak gain g_p with N. Dashed line shows that g_p can be assumed to vary linearly with N in the high-gain region.

Figure 3.1 Optical Gain of a laser diode showing gain saturation [1]

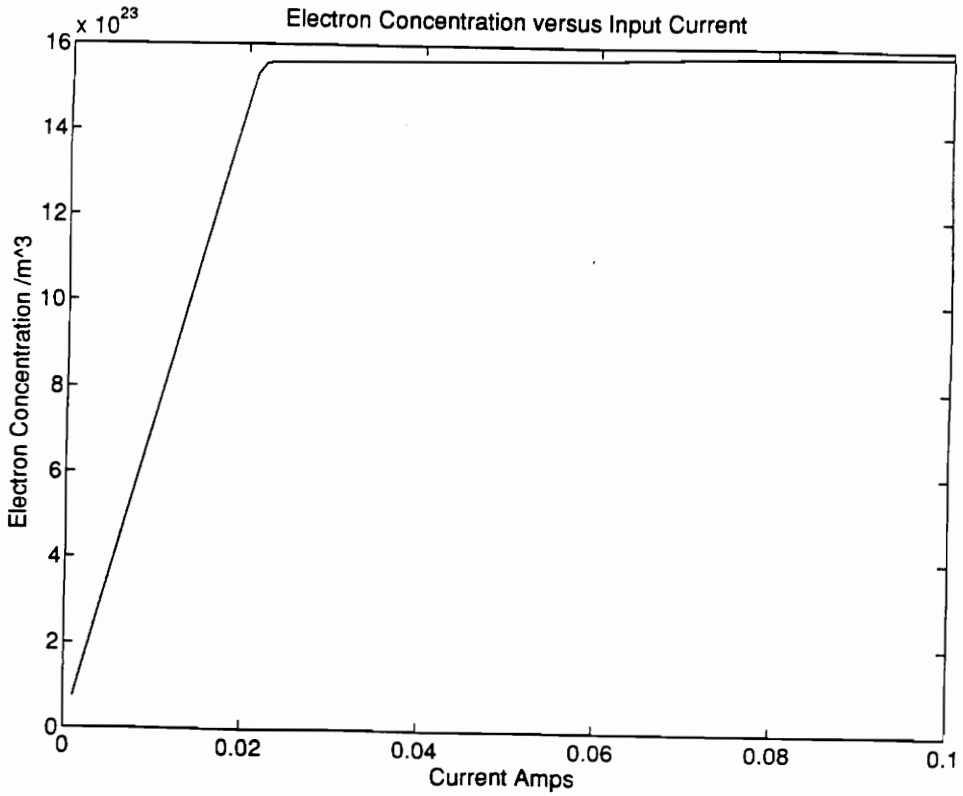

Figure 3.2 Injection Current (amperes) versus electron concentration (/m^3)

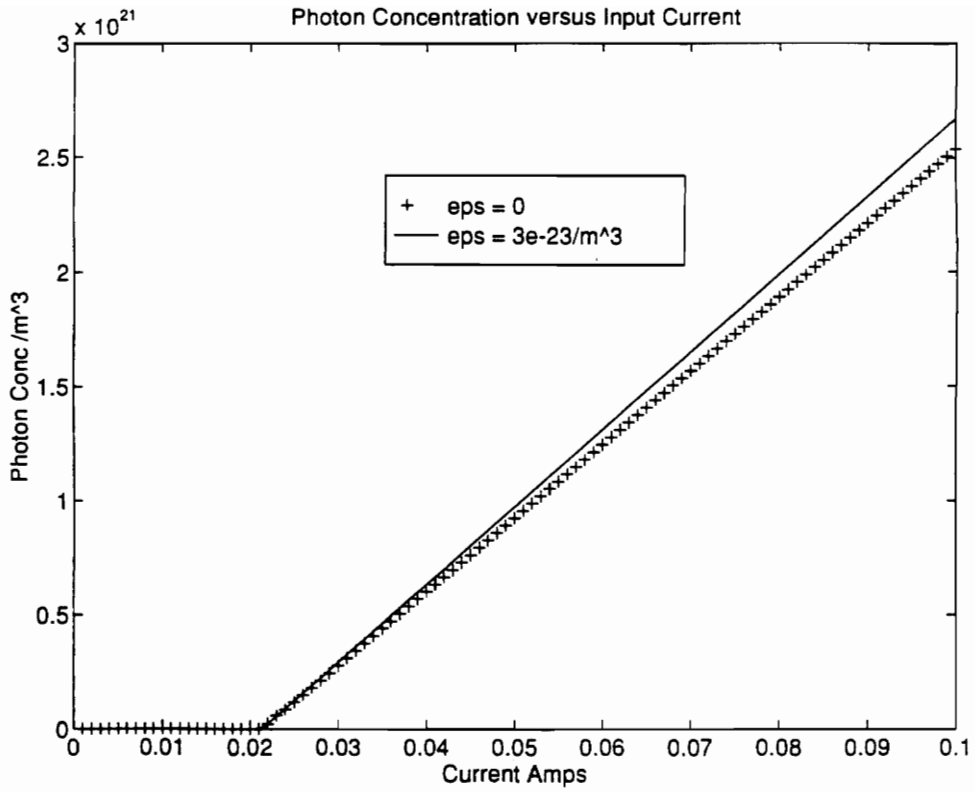

Figure 3.3 Injection Current (amperes) versus static photon concentration (/m^3)

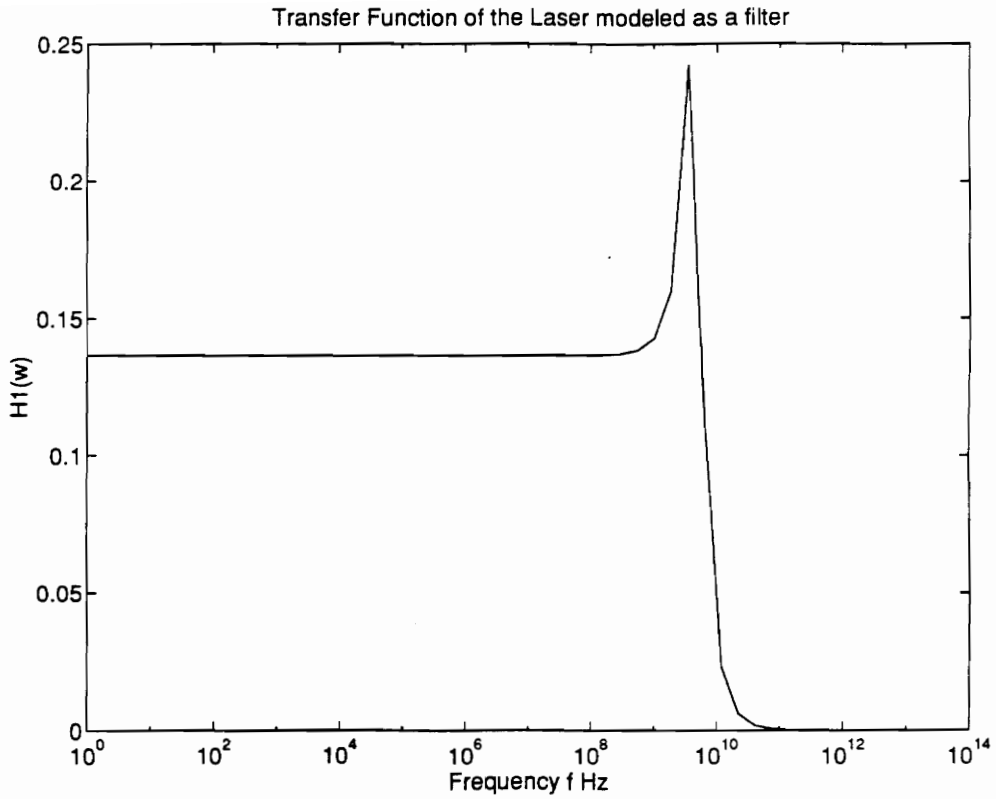

Figure 3.4 Transfer function of the laser which has been modeled as a filter

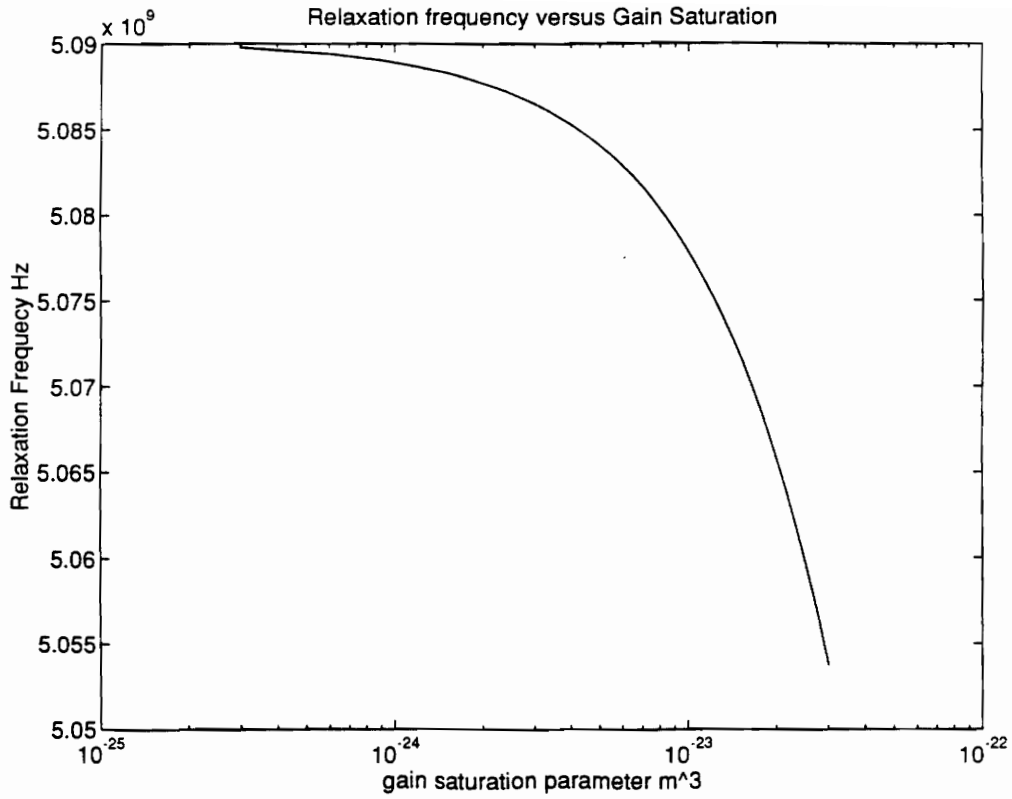

Figure 3.5 Variation of laser relaxation frequency with ε (m^3)

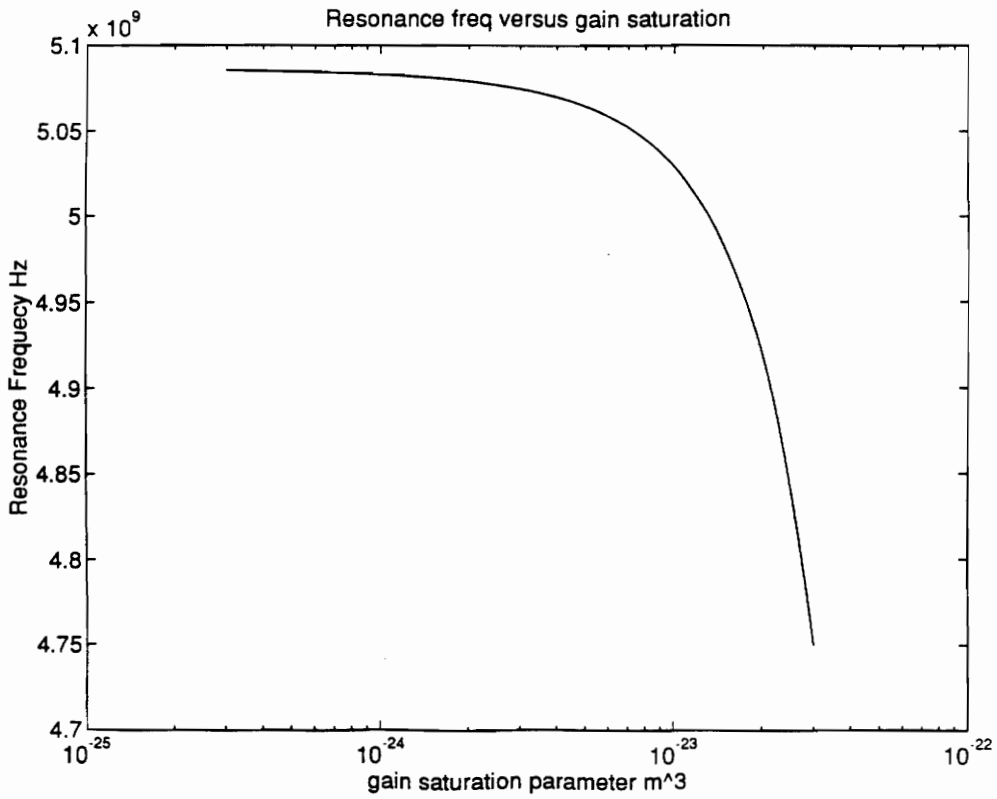

Figure 3.6 Variation of laser resonance frequency with ε (m^3)

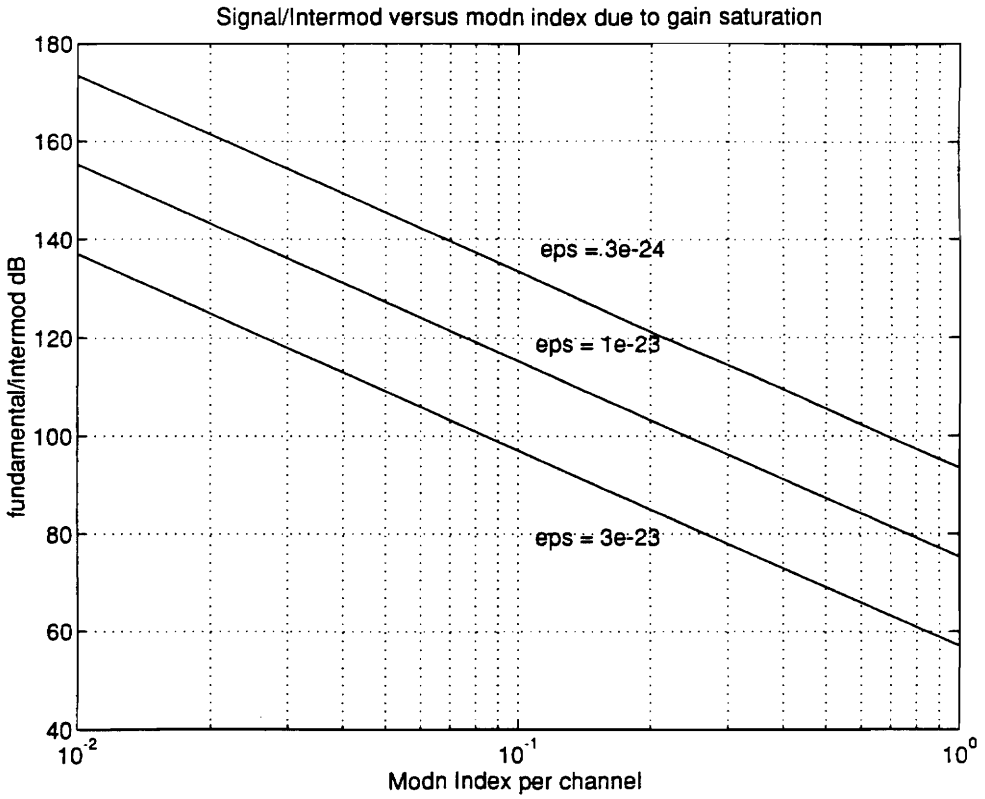

Figure 3.7 Signal to intermodulation ratio (dB) versus modn. index for various values of ε

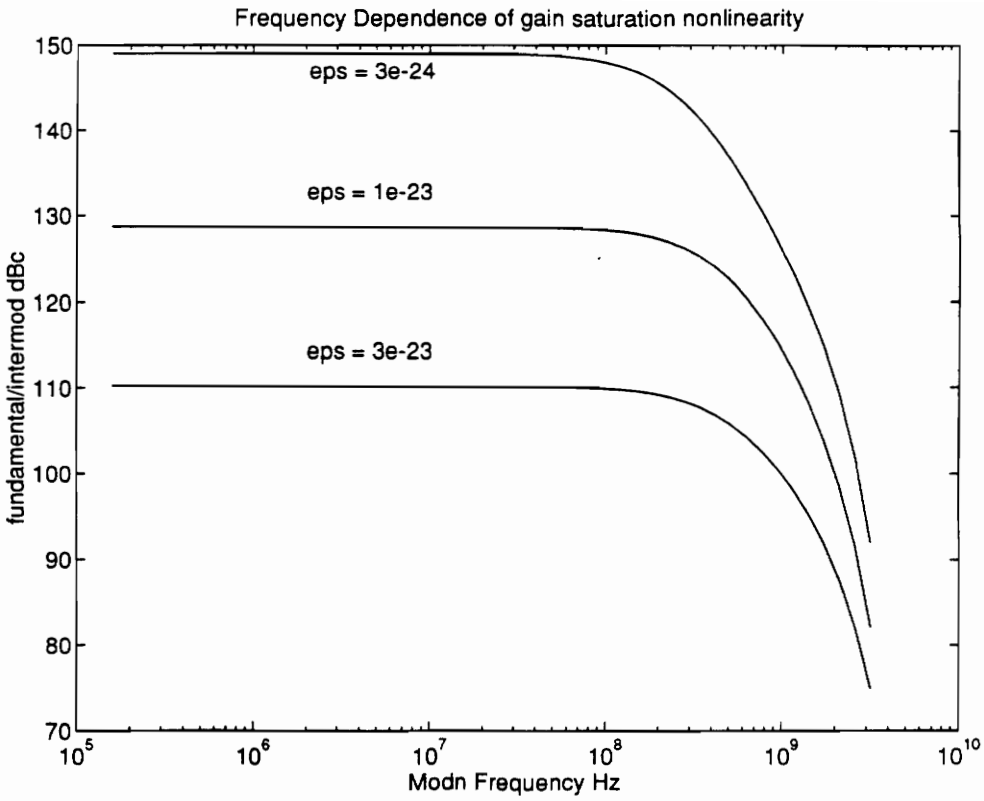

Figure 3.8 Signal to intermodulation ratio (dB) versus input frequency (Hz) for various values of ε

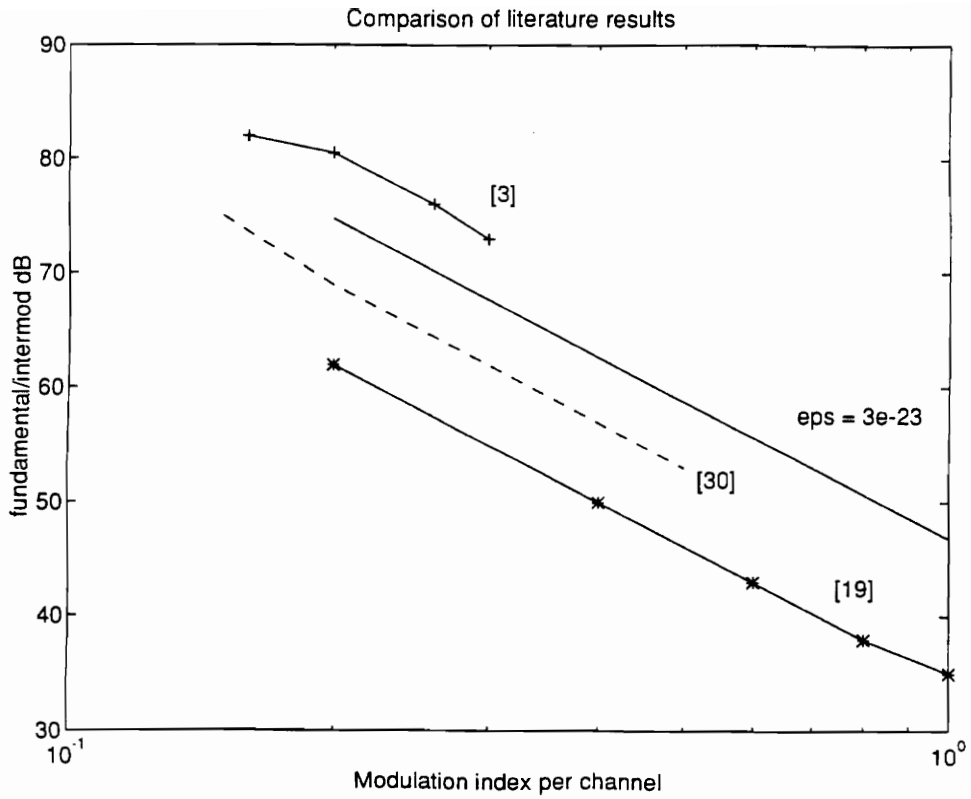

Figure 3.9 Comparison of literature results

Chapter 4.

DISPERSION AND CHIRP MODELING

One of the most significant contributors to distortion in AM-SCM systems is the combination of laser chirp and fiber dispersion. In a typical microcellular mobile environment, the distance between the micro BS and the central BS is below 10 km. But it has been shown in [18] and [24] that in the CATV environment the second order dispersion induced nonlinearity is significant even for fiber lengths as small as 10 km. It is therefore important to consider this nonlinearity for microcellular mobile application of AM-SCM systems.

In this chapter, we shall discuss the sources of this nonlinearity. We shall then proceed to model this nonlinearity to understand its dependence on dispersion, fiber length and laser chirp.

4.1 Overview of Dispersion and Chirp in AM-SCM systems

Fig. 4.1 shows the fiber link model used for to understand the behavior of the combined effect of dispersion and chirp. As we discussed in chapter 2, when the current which intensity modulates the laser is changed, it also causes a change in the optical frequency of the output. This frequency variation is called chirp. Chirp is included in fig. 4.1 as a time varying phase $\phi(t)$ which accompanies the frequency variation.

Dispersion of the fiber is modeled as a filter with a unit amplitude response and a phase response given by $\beta(\omega)z$. $\beta(\omega)$ is the propagation constant which depends on the optical frequency ω. For frequency variations much smaller than the optical frequency ω_0, we can expand $\beta(\omega)$ about ω_0 using the Taylor's series as

$$\beta(\omega)=\beta_0+\beta_1(\omega-\omega_0)+\frac{1}{2}\beta_2(\omega-\omega_0)^2+\frac{1}{6}\beta_3(\omega-\omega_0)^3+.... \quad (4.1)$$

where

$$\beta_i=\frac{d^i\beta}{d\omega^i}$$

The first two terms contribute a constant phase and a constant delay term to the optical signal. However, it is the terms $\frac{1}{2}\beta_2(\omega-\omega_0)^2+\frac{1}{6}\beta_3(\omega-\omega_0)^3+...$ which cause dispersion in the fiber and which combine with chirp to cause nonlinear distortion.

In this analysis we neglect the higher order terms of β_3, β_4, etc. as under normal operating conditions their contribution to dispersion is much smaller than the β_2 term. Consequently for the purpose of this analysis, the dispersion in the fiber is modeled as

$$H(\omega)=e^{j\frac{\beta_2 L}{2}(\omega-\omega_0)^2} \quad (4.2)$$

The term β_2 can be related to the dispersion coefficient D in the fibers as [1]

$$\beta_2=-\frac{\lambda^2}{2\pi c}D \quad (4.3)$$

where λ is the operating optical wavelength and c is the velocity of light.

4.2 Chirp Modeling

As was discussed in chapter 2, chirp depends on the linewidth enhancement parameter βc of the laser. The changes in the modulating current cause fluctuations in the intensity. These intensity fluctuations cause changes in the carrier concentration, leading to variations in the refraction index. This results in phase variations in the optical signal. The chirp is proportional to the changes in the intensity and hence is proportional to changes in the photon concentration. The laser rate equations can be modified to include chirp by including another nonlinear differential equation shown below [1]

$$\frac{d\phi}{dt}=\frac{1}{2}\beta_c\left(\Gamma\gamma(N-N_T)-\frac{1}{\tau_p}\right) \tag{4.4}$$

The frequency chirp can then be found as

$$\Delta\upsilon(t)=\frac{1}{2\pi}\frac{d\phi}{dt}=\frac{1}{4\pi}\beta_c\left(\Gamma\gamma(N-N_T)-\frac{1}{\tau_p}\right) \tag{4.5}$$

We apply the small signal modulation for an input signal consisting of three sinusoids as in chapter 3. We equate the equal frequency terms and disregard the dc terms. Then we obtain

$$\Delta\upsilon(j\omega)=\frac{\beta_c}{4\pi}\left(\Gamma\gamma\left(n_{11}(j\omega)+n_{12}(j\omega)+n_{13}(j\omega)\right)\right) \tag{4.6}$$

where γ is the differential gain, Γ is the optical confinement factor, and n_{1x} is the fundamental frequency electron concentration at the frequency ω_x.
But as was shown in the earlier chapter the fundamental electron density (n_{1x}) can be related to the photon concentration at that frequency (s_{1x}) as

$$n_{11}(j\omega)=\frac{(j\omega-D)}{C}s_{11}(j\omega) \tag{4.7}$$

where C and D are parameters of the laser which depend on the steady state condition of the laser and which were defined in chapter 3.

Using similar equations for $n_{12}(j\omega)$ and $n_{13}(j\omega)$, eqn. 4.6 is modified as

$$\Delta\upsilon(j\omega)=\frac{\beta_c}{4\pi}\left(\Gamma\gamma\frac{(j\omega-D)}{C}\left(s_{11}(j\omega)+s_{12}(j\omega)+s_{13}(j\omega)\right)\right) \tag{4.8}$$

But $s_{11}(j\omega)+s_{12}(j\omega)+s_{13}(j\omega)=s(j\omega)$ is the total photon density. We ignore the intermodulation terms that are introduced because of gain saturation. Then it follows that

$$\Delta\upsilon(j\omega)=\frac{\beta_c}{4\pi}\left(\Gamma\gamma\frac{(j\omega-D)}{C}s(j\omega)\right) \tag{4.9}$$

For the frequencies of interest between 800 MHz and 900 MHz the term (jω-D) is nearly equal to -D. Then using this equation, eqn 4.9 simplifies to

$$\Delta\upsilon(j\omega)=\frac{\beta_c}{4\pi}\left(\Gamma\gamma\frac{-D}{C}s(j\omega)\right) \tag{4.10}$$

Also as discussed earlier, the relation between photon density and optical power P(t) is

$$S(t)=\frac{2\Gamma\tau_p}{V\eta h\nu}P(t) \tag{4.11}$$

where h is the Planck's constant, η is the quantum efficiency and ν is the optical frequency.

Then using eqn's 4.10 and 4.11 we get the final result for frequency chirp as

$$\Delta\upsilon(t)=\frac{\beta_c}{4\pi}\left(\Gamma\gamma\frac{-D}{C}\frac{2\Gamma\tau_p}{V\eta h\nu}\right)P(t) \tag{4.12}$$

Thus chirp has a near linear relation with the optical intensity. We can thus model chirp as a voltage controlled oscillator where the frequency variation depends linearly on the optical intensity. By neglecting the frequency term jω in equation 4.9, we have in effect ignored any dynamic chirp in the optical signal.

4.3 Dispersion Modeling

In the earlier section, chirp was modeled as a voltage controlled oscillator. We now study how dispersion and chirp lead to nonlinearity. Specifically, we shall only consider the third order intermodulation interference, though this analysis can be carried out for second order nonlinearities also.

The optical field $E_S(t)$ at the output of the laser is given by

$$E_s(0,t)=\sqrt{P(t)}e^{-j(\omega_0 t-\phi(t))} \tag{4.13}$$

where $\phi(t)$ is the chirp introduced because of the laser and is given as

$$\phi(t)=2\pi\int \Delta\upsilon(t)dt \tag{4.14}$$

For the three signal case, the optical power can be written as

$$P(t)=P_0\left(1+\sum_{i=1}^{3} m_i \cos\omega_i t\right) \tag{4.15}$$

where m_i is the modulation index per channel. We are neglecting here the power at the intermodulation frequencies that is introduced because of gain saturation and clipping.

Now the square root in eqn 4.13 can be expanded in a power series as

$$\sqrt{P(t)}=\sqrt{P_0}\left(1+\frac{1}{2}\sum_{i=1}^{3} m_i \cos\omega_i t-\frac{1}{8}\left(\sum_{i=1}^{3} m_i \cos\omega_i t\right)^2+\frac{1}{16}\left(\sum_{i=1}^{3} m_i \cos\omega_i t\right)^3\right) \tag{4.16}$$

Here we are ignoring the terms of m_i of order 4 and above.

Also we can write

$$e^{j\phi(t)}=e^{j\frac{\beta_c A P_0}{2}\int\sum_{i=1}^{3} m_i \cos\omega_i t\,dt} \tag{4.17}$$

where $A=\Gamma\gamma\frac{-D}{C}\frac{2\Gamma\tau_p}{V\eta h\nu}$

Also we have removed all the constant terms in the expression.

Then again expanding 4.17 in a power series, we get

$$e^{j\phi(t)} = e^{j\frac{\beta_c A}{2}\sum_{i=1}^{3}\frac{m_i}{\omega_i}\sin\omega_i t}$$

$$= 1 + j\frac{\beta_c AP_0}{2}\left(\sum\frac{m_i}{\omega_i}\sin\omega_i t\right) - \frac{1}{2}\left(\frac{\beta_c AP_0}{2}\right)^2\left(\sum\frac{m_i}{\omega_i}\sin\omega_i t\right)^2 - \frac{j}{6}\left(\frac{\beta_c AP_0}{2}\right)^3\left(\sum\frac{m_i}{\omega_i}\sin\omega_i t\right)^3$$

(4.18)

Then the optical field is obtained by multiplying eqn's 4.16 and 4.18. This gives

$$E_s(0,t) = e^{-j\omega_0 t}\sqrt{P_0}\left\{1 + \sum_{i=1}^{3}\left(\frac{1}{2}m_i\cos\omega_i t + j\frac{\beta_c AP_0}{2}\frac{m_i}{\omega_i}\sin\omega_i t\right)\right.$$
$$+\cos(2\omega_1 - \omega_2)t\left(\frac{3m_1^2 m_2}{64} + \frac{1}{4}\left(\frac{\beta_c AP_0}{2}\right)^2\left(\frac{m_1^2 m_2}{4\omega_1^2} - \frac{2m_1^2 m_2}{4\omega_1\omega_2}\right)\right)$$
$$\left.-j\sin(2\omega_1 - \omega_2)t\left(\frac{1}{6}\left(\frac{\beta_c AP_0}{2}\right)^3\left(\frac{3m_1^2 m_2}{4\omega_1^2\omega_2}\right) + \left(\frac{\beta_c AP_0}{16}\right)\left(\frac{2m_1^2 m_2}{4\omega_1} - \frac{m_1^2 m_2}{4\omega_2}\right)\right)\right\}$$

(4.19)

In the above equation, we have considered only the terms at the fundamental frequency and at the intermodulation frequency ($2\omega_1 - \omega_2$).

The optical field at the output of the fiber after dispersion is given by taking the inverse Fourier transforms

$$E_{out}(L,t) = \frac{1}{2\pi}\int_{-\infty}^{\infty}E_s(\omega)H(\omega)e^{j\omega t}\,d\omega = \frac{1}{2\pi}\int_{-\infty}^{\infty}E_s(\omega)e^{j\beta(\omega)L}e^{j\omega t}\,d\omega \qquad (4.20)$$

where $E_S(\omega)$ is the Fourier Transform of $E_S(t)$, and $H(\omega) = e^{j\beta(\omega)L}$ is the transfer function of the fiber induced dispersion. If we take only the terms which cause nonlinearity, then as discussed in the section 4.1 we can take

$$H(\omega) = e^{j\frac{\beta_2 L}{2}(\omega-\omega_0)^2}$$

Using Fourier transform properties we get

$$E_{out}(L,t) = e^{-j\omega_0 t}\sqrt{P_0}\left\{1+\left(\sum_{i=1}^{3}\left(\frac{1}{2}m_i\cos\omega_i t + j\frac{\beta_c A P_0}{2}\frac{m_i}{\omega_i}\sin\omega_i t\right)e^{-j\frac{\beta_2 L}{2}\omega_I{}^2}\right)\right.$$

$$+\cos(2\omega_1-\omega_2)t\,e^{-j\frac{\beta_2 L}{2}(2\omega_1-\omega_2)^2}\left(\frac{3m_1{}^2m_2}{64}+\frac{1}{4}\left(\frac{\beta_c A P_0}{2}\right)^2\left(\frac{m_1{}^2m_2}{4\omega_1{}^2}-\frac{2m_1{}^2m_2}{4\omega_1\omega_2}\right)\right)$$

$$\left.-j\sin(2\omega_1-\omega_2)t\,e^{-j\frac{\beta_2 L}{2}(2\omega_1-\omega_2)^2}\left(\frac{1}{6}\left(\frac{\beta_c A P_0}{2}\right)^3\left(\frac{3m_1{}^2m_2}{4\omega_1{}^2\omega_2}\right)+\left(\frac{\beta_c A P_0}{16}\right)\left(\frac{2m_1{}^2m_2}{4\omega_1}-\frac{m_1{}^2m_2}{4\omega_2}\right)\right)\right\} \quad (4.21)$$

If we let

$$P=\left(\frac{3m_1{}^2m_2}{64}+\frac{1}{4}\left(\frac{\beta_c A P_0}{2}\right)^2\left(\frac{m_1{}^2m_2}{4\omega_1{}^2}-\frac{2m_1{}^2m_2}{4\omega_1\omega_2}\right)\right)$$

and

$$Q=\left(\frac{1}{6}\left(\frac{\beta_c A P_0}{2}\right)^3\left(\frac{3m_1{}^2m_2}{4\omega_1{}^2\omega_2}\right)+\left(\frac{\beta_c A P_0}{16}\right)\left(\frac{2m_1{}^2m_2}{4\omega_1}-\frac{m_1{}^2m_2}{4\omega_2}\right)\right) \quad (4.22)$$

Then the output signal is given by

$$P_{out} = \left|E_{out}E_{out}{}^*\right| \quad (4.23)$$

Using eqn's 4.21, 4.22 and 4.23 we get

$$P_{out} = \left\{ 1 + \sum_{i=1}^{3} m_i \cos\omega_i t \cos\left(\frac{\beta_2 L}{2}\omega_i^{\,2}\right) + \beta_c A P_0 \frac{m_i}{\omega_i} \sin\omega_i t \sin\left(\frac{\beta_2 L}{2}\omega_i^{\,2}\right) \right.$$
$$+ 2\cos(2\omega_1 - \omega_2)t \left(P\cos\left(\frac{\beta_2 L}{2}(2\omega_1 - \omega_2)^2\right)\right)$$
$$\left. + 2\sin(2\omega_1 - \omega_2)t \left(Q\sin\left(\frac{\beta_2 L}{2}(2\omega_1 - \omega_2)^2\right)\right)\right\} \qquad (4.24)$$

Now let us discuss the result obtained in 4.24. As has been seen, we have used the power series to expand P(t) and $e^{-j\phi(t)}$. If we put $\beta_2 = 0$ in this equation (i.e., we remove the effects of dispersion) then the nonlinearity should vanish because chirp alone cannot cause nonlinearity in the absence of dispersion. But in this case the eqn. 4.24 reduces to

$$P_{out} = P_0\left(1 + \sum_{i=1}^{3} m_i \cos\omega_i t + 2P\cos(2\omega_1 - \omega_2)t \right) \qquad (4.25)$$

We see that the nonlinearity has not completely vanished. The term that remains is a result of the error introduced in the analysis due to the power series expansions used. We can approximately compensate for this error by subtracting the nonlinear terms in (4.25) from (4.24). The validity of this approximation is a subject for further investigation. The final equation then becomes

$$P_{out} = \left\{ 1 + \sum_{i=1}^{3} m_i \cos\omega_i t \cos\left(\frac{\beta_2 L}{2}\omega_i^{\,2}\right) + \beta_c A P_0 \frac{m_i}{\omega_i} \sin\omega_i t \sin\left(\frac{\beta_2 L}{2}\omega_i^{\,2}\right) \right.$$
$$\left. + 2\sin(2\omega_1 - \omega_2)t \left(Q\sin\left(\frac{\beta_2 L}{2}(2\omega_1 - \omega_2)^2\right)\right)\right\} \qquad (4.26)$$

We use this expression for the further discussions.

4.4 Behavior of the nonlinearity with various physical parameters.

In this section we consider the change in the nonlinearity caused by changing the linewidth enhancing parameter, the length of the fiber and the modulation index. The wavelength of

the optical signal used is 1.3μm and the dispersion coefficient of the fiber is taken as 1.3ps/(km.nm). The frequency of the modulating signals are ω_1 = 800 MHz and ω_2 = 825 MHz.

Figure 4.2 shows the dependence of the nonlinearity on the modulation index per channel plotted for various gain saturation parameters ε. The linewidth enhancing factor of the laser is taken to be 5 and the length of the fiber is 5 km.. As we can see, there is an increase in the nonlinearity as the modulation index per channel increases. Again, an increase in the modulation index by a factor of 10 causes a 40 dB decrease in the signal to interference ratio. This behavior is similar to the gain saturation nonlinearity as was discussed in chapter 3. Also increase in the gain saturation parameters causes an increase in the nonlinearity. This behavior can be explained by the fact that the two modulating signals are close to the resonance frequency of the laser. As a result the D and C laser parameters are extremely susceptible to changes in gain saturation. This causes increased nonlinearity at higher ε.

Figure 4.3 shows the relation between the nonlinearity and the length of the fiber. The linewidth enhancement factor is again taken as 5 and the modulation index per channel is fixed at 2%. The signal to intermodulation ratio decreases by 20 dB for an increase in the length of the fiber by a factor of 10 and hence the signal to intermodulation ratio is inversely proportional to L^2. The effect of dispersion becomes more pronounced as the length of the fiber increases. It is interesting to note that even for small fiber lengths the nonlinearity is significant. Thus even for small lengths as would be encountered in a typical microcellular environment, it is important to take into account this type of nonlinearity.

Figure 4.4 describes the relation between the nonlinearity and the linewidth enhancement factor of the laser. As the linewidth enhancement factor increases, its relation with the signal to interference slowly deviates from a linear relationship . The linewidth enhancing factor is linearly related to the spectral linewidth of the laser [1]. The modulation index per channel used is 2% and the length of the fiber is 5 km. The value of the gain saturation parameter used is $3(10)^{-23}$. As the linewidth enhancement factor increases, the chirping increases, causing stronger nonlinearity.

In fig. 4.5, we investigate the variation of nonlinearity against the combined variation of linewidth enhancement factor and the length of the fiber. The other parameters remain the same. We plot nonlinearity against the product $\beta_2 L \beta_c$. Then as β_c has a linear relation with the spectral linewidth of the laser [1], the product is linearly related to the total dispersion in the fiber. As may be expected, as the dispersion in the fiber increases, the nonlinearity increases. From this figure, we observe that the nonlinearity is not completely characterized by $\beta_2 L \beta_{c,}$, as for a single value of $\beta_2 L \beta_{c,}$, the nonlinearity can take differing values. Upon analyzing eqn 3.2.26, we found that the parameter which nearly independently gave a unique value of nonlinearity was $\beta_2 L \beta_c^2$. The variation of the intermod strength to $\beta_2 L \beta_c^2$ is shown in fig. 4.6. Note that for a given value of $\beta_2 L \beta_c^2$ the variation of the nonlinearity is extremely small compared to fig. 4.5.

We can also draw an interesting conclusion by comparing the results obtained in this section and the previous section on gain saturation. We see that in the mobile environment, the nonlinearity caused because of the dispersion and chirp is comparable to that caused by the gain saturation. We can suppress this nonlinearity by operating very close to the dispersion minimum. However as we note, even a slight shift in the dispersion coefficient can cause significant degradation in the performance.

4.5 Conclusions

In this chapter, we discussed the effect of dispersion and chirp nonlinearity on the system performance. We also inferred that under the mobile conditions, dispersion and chirp nonlinearity is comparable to the the gain saturation nonlinearity. We saw the dependence of the distortion on the modulation index per channel, the length of the fiber and the linewidth enhancement factor of the laser. These results are (we believe) new, since related work in the literature is for CATV applications where second-order distortion effects are dominant.

In the next chapters, we shall discuss the noise analysis in fiber links. We shall then combine the results obtained for the nonlinearity and the noise to find the dynamic range for the mobile signals.

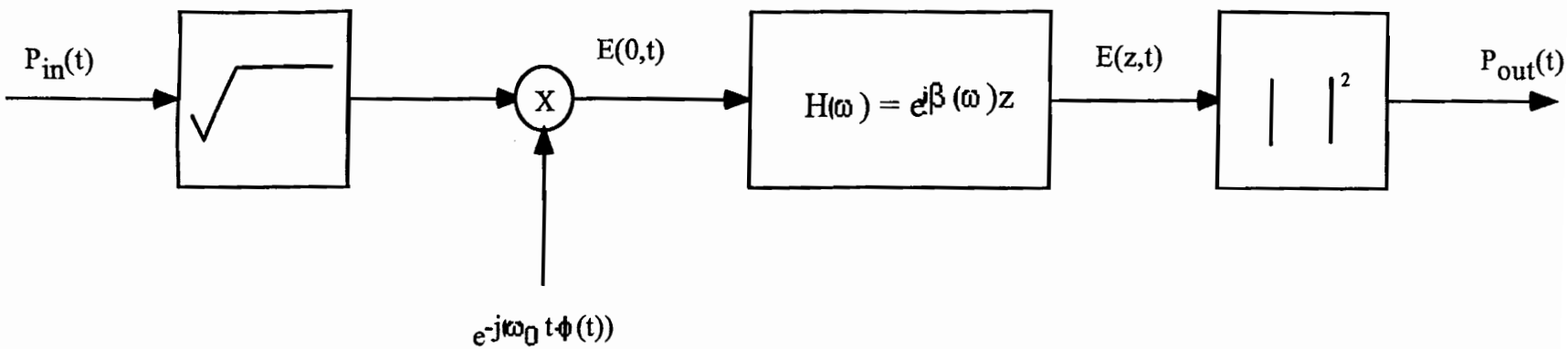

Figure 4.1 Fiber Dispersion and Chirp Model

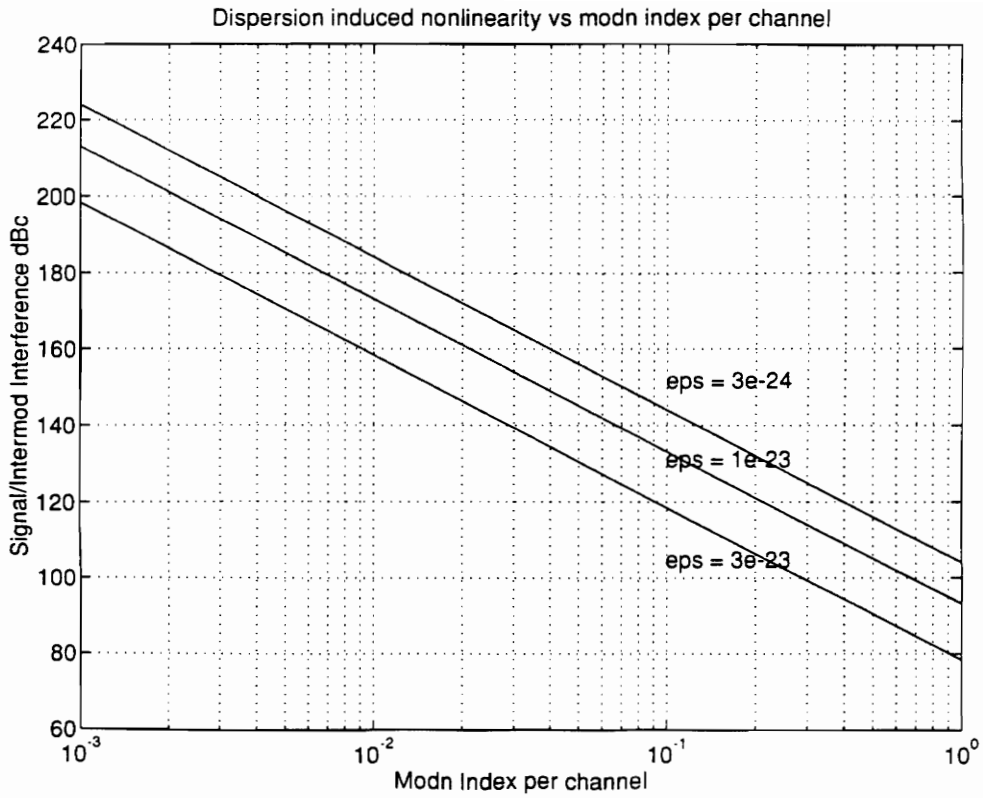

Figure 4.2 Variation of signal to interference ratio (dB) with modn. index per channel

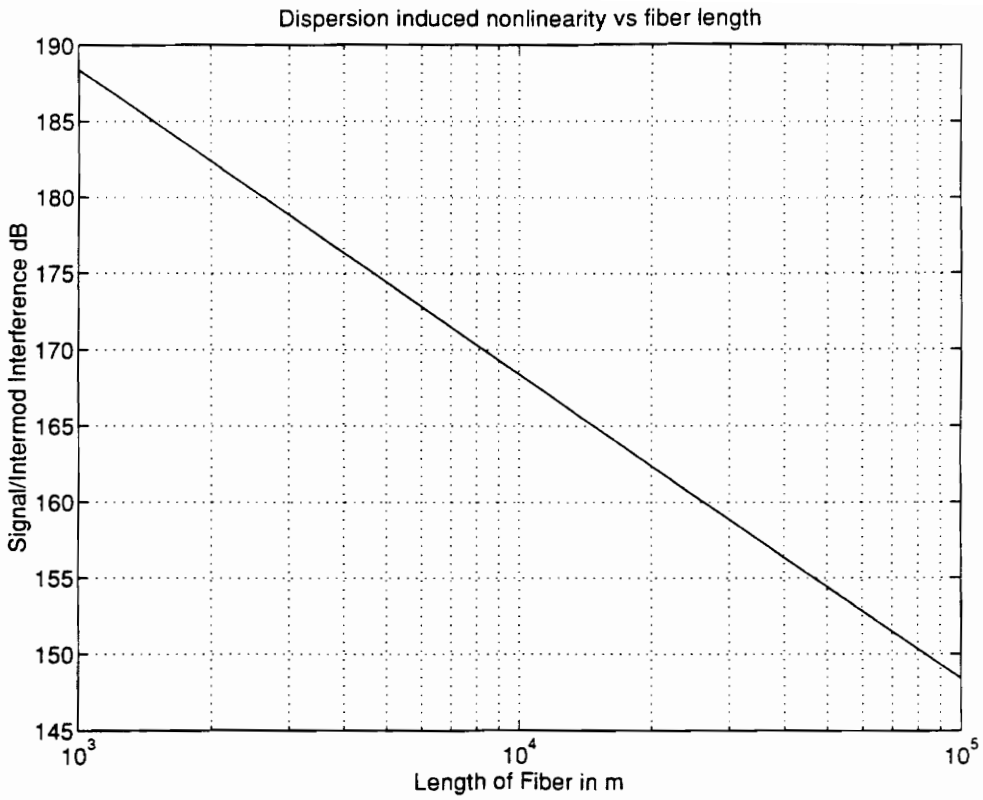

Figure 4.3 Variation of the signal to intermodulation ratio (dB) with length of the fiber (m)

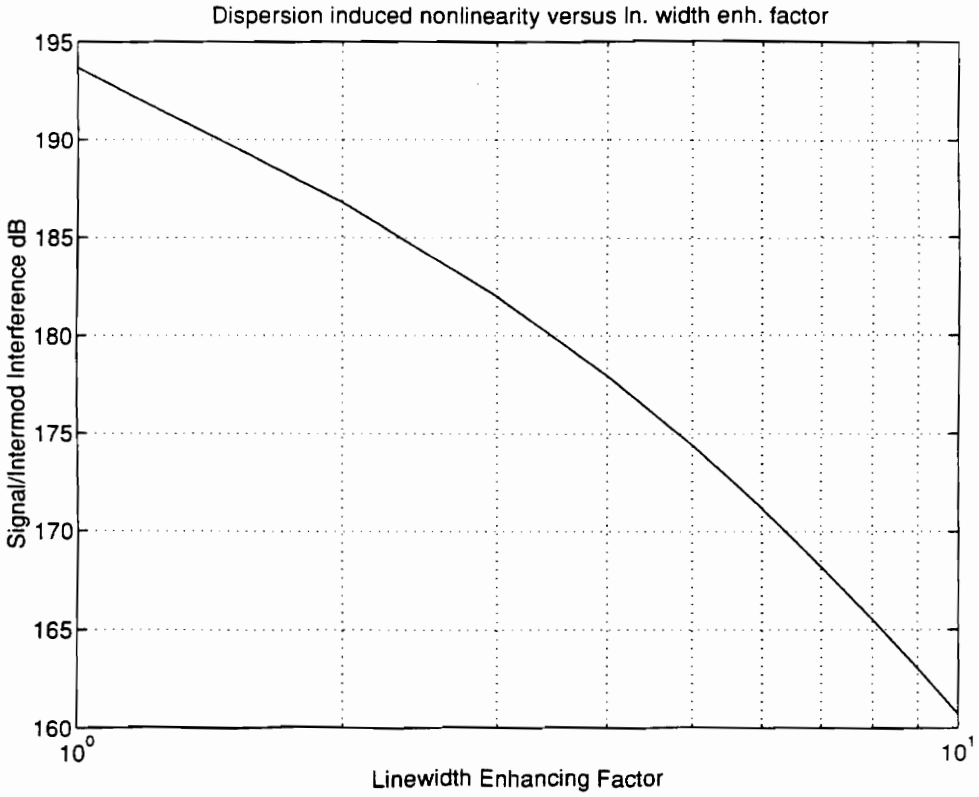

Figure 4.4 Variation of signal to intermodulation ratio (dB) with linewidth enhancing factor β_c

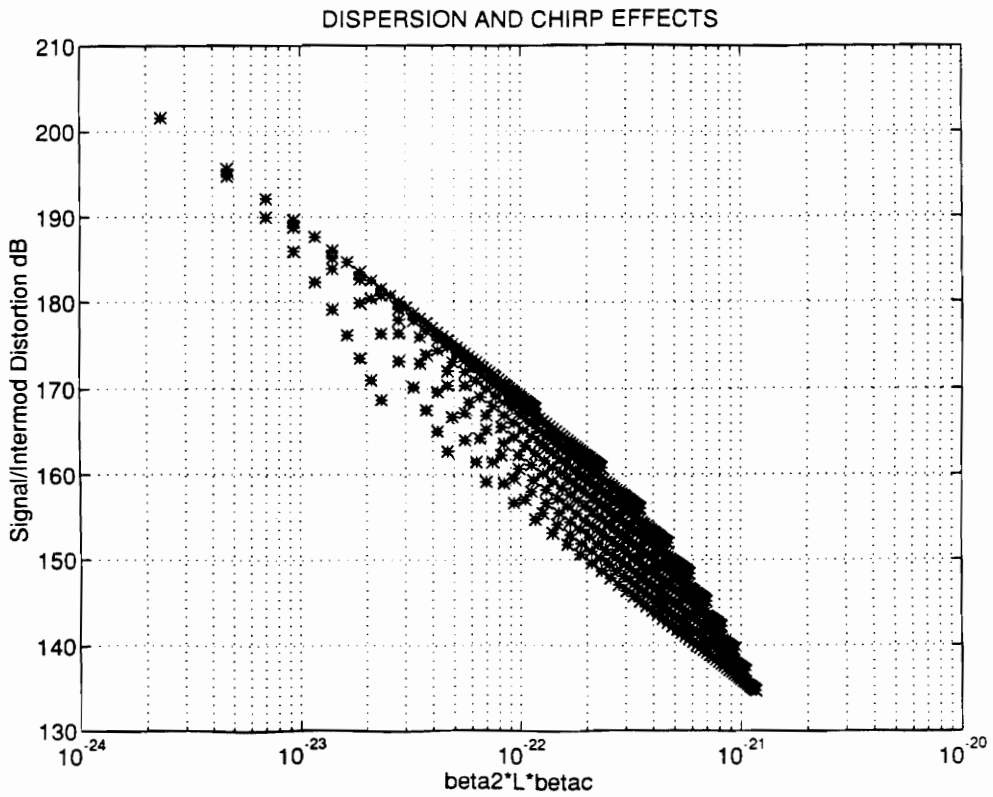

Figure 4.5 Variation of signal to intermodulation ratio (dB) with $\beta_2 L \beta_c$

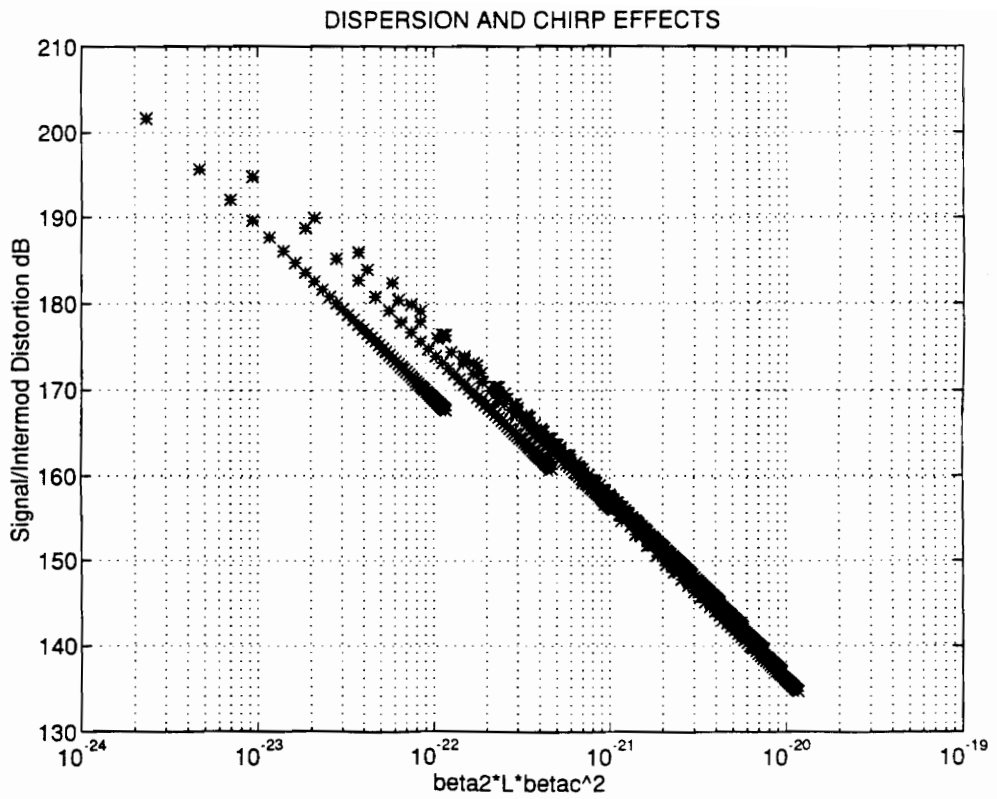

Figure 4.6 Variation of signal to intermodulation ratio (dB) with $\beta_2 L \beta_c^2$

Chapter 5.

PERFORMANCE OF MOBILE SIGNALS IN THE PRESENCE OF FIBER LINK NOISE

In chapter 2 we discussed the major noise sources in the fiber links that are used to transmit analog signals. We saw that the sources of noise are shot noise, thermal noise, and laser RIN. Analog fiber optic systems have stringent noise requirements . The maximum signal to noise ratio that can be obtained from the fiber link is limited by the RIN noise.

In this chapter, we shall analyze the signal to noise ratio (SNR) that can obtained from the fiber link carrying AMPS FM signals. We shall also investigate the bit error rate (BER) for TDMA signals when they are sent over the fiber.

5.1 Noise in AMPS FM signals

As discussed in chapter 1, AMPS uses the frequency spectrum between 824 MHz and 849 MHz for the uplink channels and the frequencies between 869 MHz and 894 MHz for the downlink signals. Each channel uses 30 KHz bandwidth. The peak deviation for the voice channels (ΔF) is $\pm$ 12 KHz. The frequency modulation index (β) is approximately 3.

In this analysis we extend the noise analysis to FM signals, including the noise introduced by the fiber optics system. This analysis is the extension of the standard FM improvement formula to our system. Let us consider a simple block diagram shown in figure 5.1.

Now we can write the output of the FM transmitter as

$$s_1(t) = A_c \cos\left(\omega_c t + D_f \int_{-\infty}^{t} i(x)dx \right) \tag{5.1}$$

where A_C is the amplitude of the carrier, ω_C is the radio carrier frequency, D_f is the frequency deviation constant that has units of radians/volt.sec and i(x) is the information signal. The FM modulation is implemented at an intermediate frequency and the signal is then translated to the carrier frequency.

Now as this signal passes over the mobile channel, background noise which is assumed to be gaussian distributed is added to the signal. We ignore the effects of multipath fading in this analysis. Then the signal that is received at the micro BS can be written as

$$s_2(t) = A_c \cos\left(\omega_c t + D_f \int_{-\infty}^{t} i(x)dx \right) + n(t) \tag{5.2}$$

where n(t) is the background noise. Over the relatively small bandwidth of the AMPS signal, the noise can be expressed as $n(t) = x_n(t)\cos\omega_c t - y_n(t)\sin\omega_c t$ where $x_n(t)$ and $y_n(t)$ are quadrature components and $x_n(t) + jy_n(t) = g(t)$ where g(t) is the complex envelope of the gaussian noise n(t)[28]. The power spectral density of this noise can be assumed to be uniform over the bandwidth of the signal and is expressed as

$$P_n(f) = \frac{N_0}{2} \tag{5.3}$$

In this situation the individual power spectral densities of the quadrature components are related as [28]

$$P_{x_n}(f) = P_{y_n}(f) = P_n(f - f_c) + P_n(f + f_c) \tag{5.4}$$

The sum of such signals from various mobiles is received at the base station and is used to modulate the laser. But before the intensity modulation process, the amplitude of this signal is scaled so that the modulation index of the laser per channel does not exceed the predetermined value m. Let us assume that there are n signals arriving at the base station. Let A_{ctotal} be the average of the signal strength of one individual channel. We assume that over a period of time all the channels will have approximately the same average signal strength and hence A_{ctotal} will be the same for all channels. We scale the signal such that an individual signal strength of A_{ctotal} causes a modulation index per channel m. Then we can write the equation for the signal that intensity modulates the laser as

$$s_3(t)=\frac{mP_0}{A_{ctotal}}s_2(t)=\frac{mP_0}{A_{ctotal}}\left(A_c\cos\left(\omega_c t+D_f\int_{-\infty}^{t}i(x)dx\right)+x_n(t)\cos\omega_c t-y_n(t)\sin\omega_c t\right) \tag{5.5}$$

The intensity modulated optical signal is then transmitted over the fiber. It is corrupted by the various noise sources of the fiber link. It is detected by the photodetector. Let $\Re$ be the responsivity of the photodetector. The detected signal can be expressed as

$$s_4(t)=A_c\frac{m\Re P_0}{A_{ctotal}}\cos\left(\omega_c t+D_f\int_{-\infty}^{t}i(x)dx\right)+x_n(t)\frac{m\Re P_0}{A_{ctotal}}\cos\omega_c t$$

$$-y_n(t)\frac{m\Re P_0}{A_{ctotal}}\sin\omega_c t+n_{nf}(t) \tag{5.6}$$

where $n_{nf}(t)$ is the bandlimited noise that is introduced by the fiber optic system. This noise consists of the thermal noise, shot noise and the laser RIN. The total noise can be assumed to be Gaussian in nature. This assumption is particularly valid over the relatively small bandwidth of our channel. Then as earlier we can express the noise as a sum of two quadrature components $n_{nf}(t)=x_{nf}(t)\cos\omega_c(t)-y_{nf}(t)\sin\omega_c t$.

Then using this modification, we can modify eqn. 5.6 as

$$s_4(t)=A_c\frac{m\Re P_0}{A_{ctotal}}\cos\left(\omega_c t+D_f\int_{-\infty}^{t}i(x)dx\right)+x_n(t)\frac{m\Re P_0}{A_{ctotal}}\cos\omega_c t$$

$$-y_n(t)\frac{m\Re P_0}{A_{ctotal}}\sin\omega_c t+x_{nf}(t)\cos\omega_c t-y_{nf}(t)\sin\omega_c t \qquad (5.7)$$

As we have assumed the noise introduced by the fiber optic link is white gaussian noise, we can express the power spectral density of this noise as

$$P_{nf}(f)=\frac{1}{2}\left(<i_{th}^{\ 2}>+2q\Re P_0+rin(\Re P_0)^2\right)R_L \qquad (5.8)$$

where $<i_{th}^2>$ is the receiver thermal noise spectral density, q is the electron charge, rin is the RIN of the laser, P_0 is the received optical power and R_L is the receiver load resistance. The term $<i_{th}^2>$ originates from the thermal noise, shot noise is represented by $2q\Re P_0$ and the laser RIN is included through the term $rin(\Re P_0)^2$.

It is this signal that is received at the FM detector. The FM detector consists of a bandpass filter, a differentiator and an envelope detector. The structure of the FM detector is shown in the figure 5.2

Then we can write eqn. 5.7 as

$$v_1(t)=s_4(t)=A_c\frac{m\Re P_0}{A_{ctotal}}\cos\left(\omega_c t+D_f\int_{-\infty}^{t}i(x)dx\right)+x_n(t)\frac{m\Re P_0}{A_{ctotal}}\cos\omega_c t$$

$$-y_n(t)\frac{m\Re P_0}{A_{ctotal}}\sin\omega_c t+x_{nf}(t)\cos\omega_c t-y_{nf}(t)\sin\omega_c t \qquad (5.9)$$

The differentiator output is given by

$$v_2(t)=-A_cD_fi(t)\frac{m\Re P_0}{A_{ctotal}}\sin\left(\omega_c t+D_f\int_{-\infty}^{t}i(x)dx\right)+\frac{m\Re P_0}{A_{ctotal}}\cos\omega_c t\frac{dx_n}{dt}$$

$$-x_n(t)\omega_c\frac{m\Re P_0}{A_{ctotal}}\sin\omega_c t-\frac{m\Re P_0}{A_{ctotal}}\sin\omega_c t\frac{dy_n}{dt}-y_n(t)\omega_c\frac{m\Re P_0}{A_{ctotal}}\cos\omega_c t$$

$$-x_{nf}(t)\omega_c \sin\omega_c t + \frac{dx_{nf}}{dt}\cos\omega_c t - y_{nf}(t)\omega_c \cos\omega_c t - \frac{dy_{nf}}{dt}\sin\omega_c t \quad (5.10)$$

If we use a balanced modulator so that all the ω_C terms vanish then eqn. 5.10 reduces to

$$v_2(t) = -A_c D_f i(t)\frac{m\Re P_0}{A_{ctotal}}\sin\left(\omega_c t + D_f\int_{-\infty}^{t} i(x)dx\right) + \frac{m\Re P_0}{A_{ctotal}}\cos\omega_c t\frac{dx_n}{dt}$$

$$-\frac{m\Re P_0}{A_{ctotal}}\sin\omega_c t\frac{dy_n}{dt} + \frac{dx_{nf}}{dt}\cos\omega_c t - \frac{dy_{nf}}{dt}\sin\omega_c t \quad (5.11)$$

If we assume $D_f\int_{-\infty}^{t} i(x)dx = 0$, then the eqn. 5.11 reduces to

$$v_2(t) = -A_c D_f i(t)\frac{m\Re P_0}{A_{ctotal}}\sin\omega_c t + \frac{m\Re P_0}{A_{ctotal}}\cos\omega_c t\frac{dx_n}{dt}$$
$$-\frac{m\Re P_0}{A_{ctotal}}\sin\omega_c t\frac{dy_n}{dt} + \frac{dx_{nf}}{dt}\cos\omega_c t - \frac{dy_{nf}}{dt}\sin\omega_c t \quad (5.12)$$

For a signal of the type a(t)cosωt - b(t)sinωt, the output of the envelope detector is $\sqrt{a(t)^2 + b(t)^2}$

Thus the output of the envelope detector in this case is

$$v_3(t) = \sqrt{\left(A_c D_f i(t)\frac{m\Re P_0}{A_{ctotal}} + \frac{dy_n}{dt}\frac{m\Re P_0}{A_{ctotal}} + \frac{dy_{nf}}{dt}\right)^2 + \left(\frac{dx_n}{dt}\frac{m\Re P_0}{A_{ctotal}} + \frac{dx_{nf}}{dt}\right)^2} \quad (5.13)$$

If we assume that the signal strength is much stronger than noise power, then

$$\left(\frac{dx_n}{dt}\frac{m\Re P_0}{A_{ctotal}} + \frac{dx_{nf}}{dt}\right)^2 << \left(A_c D_f i(t)\frac{m\Re P_0}{A_{ctotal}} + \frac{dy_n}{dt}\frac{m\Re P_0}{A_{ctotal}} + \frac{dy_{nf}}{dt}\right)^2 \quad (5.14)$$

Thus $v_3(t)$ in eqn. 5.13 can be further reduced to

$$v_3(t) = s_{out}(t) = \left(A_c D_f i(t) \frac{m\Re P_0}{A_{ctotal}} + \frac{dy_n}{dt} \frac{m\Re P_0}{A_{ctotal}} + \frac{dy_{nf}}{dt} \right) \tag{5.15}$$

Then the SNR is given as

$$SNR = \frac{\left(A_c D_f \frac{m\Re P_0}{A_{ctotal}} \right)^2 \overline{i(t)^2}}{\left(\frac{m\Re P_0}{A_{ctotal}} \right)^2 \overline{\left(\frac{dy_n(t)}{dt} \right)^2} + \overline{\left(\frac{dy_{nf}(t)}{dt} \right)^2}} \tag{5.16}$$

We can implement a differentiator as a filter with transfer function

$$H(f) = j(2\pi f) \tag{5.17}$$

Then the power spectral density of the differentiated signal can be related to that of the original signal by the relation

$$P_{\frac{dy_n}{dt}}(f) = P_{y_n}(f)\left|H(f)\right|^2 = P_{y_f}(f)(2\pi f)^2 \tag{5.18}$$

Then the noise power is given as

$$N = \left(\frac{m\Re P_0}{A_{ctotal}} \right)^2 \int_{-B}^{B} P_{\frac{dy_n}{dt}} df + \int_{-B}^{B} P_{\frac{dy_{nf}}{dt}} df = \left(\frac{m\Re P_0}{A_{ctotal}} \right)^2 \int_{-B}^{B} (2\pi f)^2 P_{y_n}(f) df + \int_{-B}^{B} (2\pi f)^2 P_{y_{nf}}(f) df \tag{5.19}$$

Integrating this equation and substituting in (5.16), and using eqns (5.3), (5.4) and (5.8) we get the final signal to noise ratio as

$$SNR = \frac{\left(\frac{A_c m\Re P_0}{A_{ctotal}} D_f \right)^2 \overline{i(t)^2}}{\left(\frac{m\Re P_0}{A_{ctotal}} \right)^2 \left(\frac{8\pi^2 B^3 N_0}{3} \right) + \left(\frac{8\pi^2 B^3}{3} \frac{1}{2} \left(rin\left(\Re P_0\right)^2 + 2q\Re P_0 + < i_{th}^{\ 2} > \right) R_L \right)} \tag{5.20}$$

Substituting $D_f = \frac{2\pi B\beta}{V_p}$, where V_p is the maximum value of the information signal i(t), we get the final expression as

$$SNR = \frac{\left(\frac{A_c m\Re P_0}{A_{ctotal}}\right)^2 \frac{\overline{i(t)^2}}{V_p^2} 4\pi^2 B^2 \beta^2}{\left(\frac{m\Re P_0}{A_{ctotal}}\right)^2 \left(\frac{8\pi^2 B^3 N_0}{3}\right) + \left(\frac{8\pi^2 B^3}{3}\frac{1}{2}\left(rin(\Re P_0)^2 + 2q\Re P_0 + < i_{th}^2 >\right)R_L\right)} \tag{5.21}$$

We shall use this equation for further analysis.

5.2 BER Analysis for TDMA signals

The IS 54 (TDMA) digital standard for mobile communications uses a speech coder which digitally encodes the voice at 7.95 Kb/s. A new digital modulation technique, π/4 DQPSK is used for modulating the output from the speech coder. The π/4 DQPSK is a 4-ary modulation technique using 2 bits per symbol. It can be received using an incoherent receiver and does not require the regeneration of the in phase carrier signal at the receiver. The symbol to be transmitted depends on the earlier symbol that was transmitted. The phase difference between the present aand the previous symbols depends on the bits that are to be transmitted by the present symbol.

The BER for π/4 DQPSK in channels which are relatively slow fading can be closely approximated by the BER relation for DPSK.

Then the BER for TDMA can be approximated by [29]

$$BER = \frac{1}{2}e^{-\gamma} \tag{5.22}$$

where γ is the CNR.

In our application, the two sources of noise are again the background noise introduced in the RF channel and the fiber link introduced noise. Then the final CNR at the receiver is given by

$$\frac{1}{CNR_{final}} = \frac{1}{CNR_{background}} + \frac{1}{CNR_{fiberlink}} \tag{5.23}$$

The Carrier to Noise Ratio (CNR) per channel of the fiber link is given by

$$CNR = \frac{\frac{1}{2} m^2 \Re^2 P_0^2}{rin \Re^2 P_0^2 B + 2q\Re P_0 B + < i_{th}^2 > B} \tag{5.24}$$

where m is the modulation index per channel, rin is the RIN of the laser, $\Re$ is the responsivity of the photodetector, P_0 is the average received power, B is the bandwidth of the signal, $<i_{th}>^2$ is the thermal noise spectral density and q is the electron charge.

Equations 5.22-5.24 are used to evaluate the BER for TDMA signals.

5.3 Numerical Results

In fig. 5.3, the relation between the SNR of the AMPS system and the input electrical power to the laser is calculated from eqn 5.21 for two values of N_0. The power spectral density of $N_0 = 10^{-10}$ corresponds to a SNR of 22 dB at the output of the FM detector in the absence of the fiber link, whereas $N_0 = 10^{-12}$ corresponds to a SNR of 42 dB at the output of the FM detector in the absence of the fiber link. As can be seen from these plots, at low incoming powers, the noise introduced by the fiber link is dominant and causes significant degradation of SNR. Change in the incoming power does not cause any change in the performance limitation due to the background noise. As the input power increases, it causes an increase in the modulation index of the channel as is obvious from equation 5.24. The SNR increases with increase in the input power. At this stage, the background noise starts dominating and limits the maximum available SNR from the system.

In these calculations, we have assumed that $\frac{\overline{i(t)^2}}{V_p^2} = 0.5$ (as is the case for sinusoidal modulation). Also, the power of the individual FM signal received at the base station (i.e., $A_c^2/2$) is -70dBm and the total power in the combined signal (i.e., $A_{ctotal}^2/2$) is -40 dBm.

In figure 5.4, we plot the BER of the TDMA system as can be calculated from eqns 5.22 to 5.24 against the input power. There is a strong similarity in the nature of this plot and the earlier plot involving the analog FM signal. In the two cases for which we have plotted the results, the CNR of the incoming signals is different. As is obvious from the plots, at low input powers, the noise that is introduced by the fiber link is stronger than the noise in the original signal and the fiber noise dominates to increase the BER. As the input power increases, it causes a corresponding increase in the modulation index of that channel, which causes an increase in the CNR of the fiber link. Again as in the analog case, ultimately the background noise dominates and thus the minimum BER that is possible is limited by the CNR of the incoming signal. Also as the background noise increases, the minimum BER that is possible from the system increases correspondingly.

In these calculations, $\Re$ = 0.93 mA/mW, $\sqrt{< i_{th}^2 >}$ = 7pA/Hz, laser RIN is -150dB/Hz, the received power is P0 = 1mW, and the relation between the modulation index and the input power (P_{in}) is

$$P_{in} = (I_B - I_{TH})m^2 R_{laser} \qquad (5.25)$$

where I_B is the bias current of the laser (= 40mA), I_{TH} is the threshold current of the laser (= 20mA) and R_{laser} is the input resistance of the laser (=50Ω).

If we compare the fig. 5.3b (analog FM) and the lower curve of the fig. 5.4, we see that the background noise in both cases causes the maximum signal to noise ratio of 20 dB. In both cases, the background noise starts dominating at nearly the same input power range (around -100 dBW). Thus, we see that the noise / BER performance of both the FM and the TDMA systems is comparable in the absence of any fading.

5.4 Summary

In this chapter, we analyzed the performance of the mobile signals in the combined presence of fiber noise and background noise introduced by the RF channel. We saw that at low input powers, the fiber link noise dominates over the background noise, but the best performance is

limited by the background noise. Also the behavior of the AMPS and TDMA signals is comparable in the absence of any fading.

In the next chapter, we shall combine the results from this chapter to the nonlinearity models developed in chapters 3 and 4 to find the dynamic range available from the fiber link for the mobile signals.

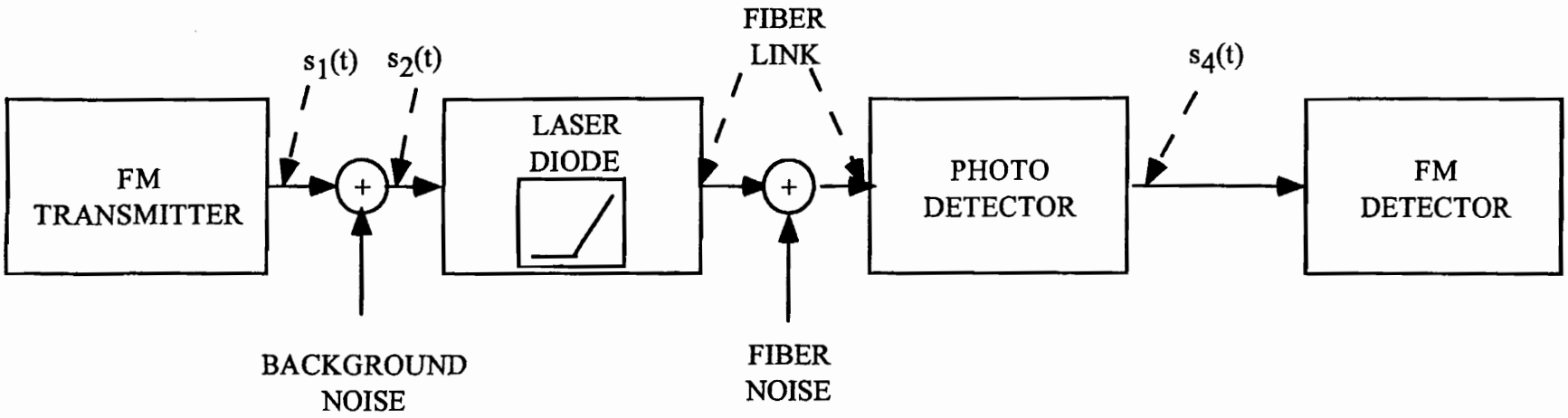

Figure 5.1 Simplified block diagram with the sources of noise

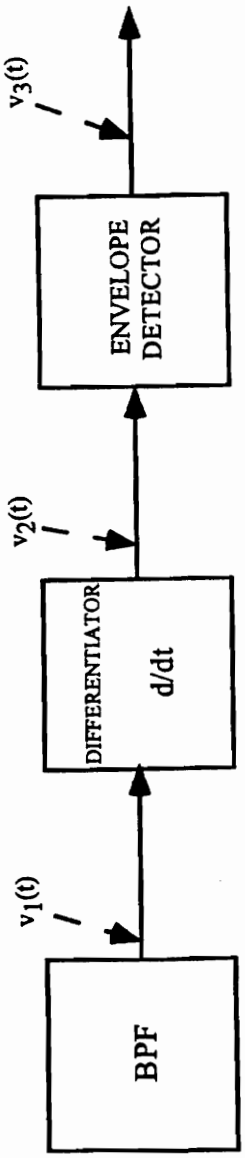

Figure 5.2 FM DETECTOR

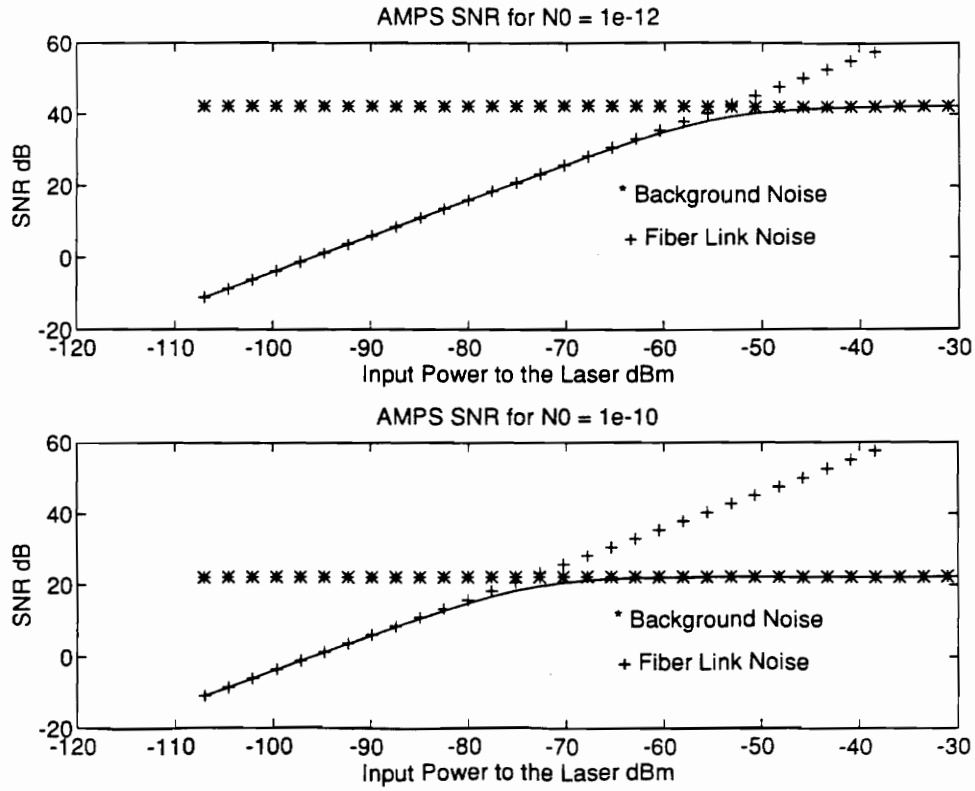

Figure 5.3 AMPS SNR variation with received power for a) $N_0 = 10^{-10}$ and b) $N_0 = 10^{-12}$

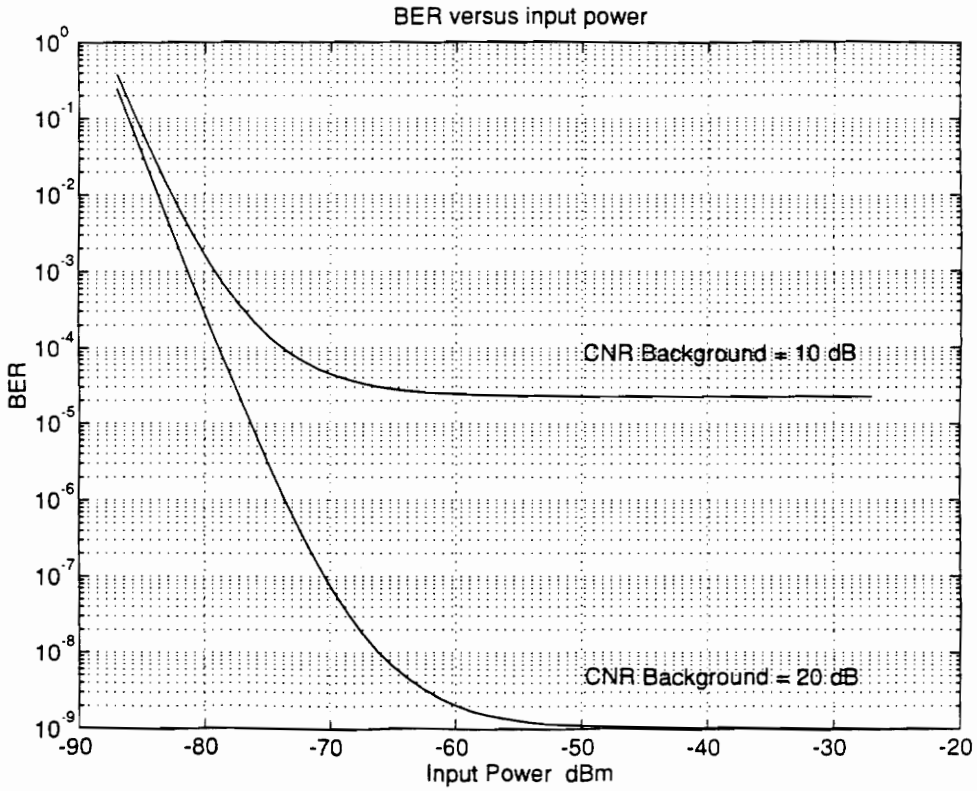

Figure 5.4 TDMA BER variation with input power for a) $CNR_{background}$ = 10dB and b) $CNR_{background}$ = 20 dB

Chapter 6.

DYNAMIC RANGE OF MOBILE SIGNALS

In chapters 3 and 4 we developed the models for the major sources of nonlinearity, namely gain saturation and dispersion and chirp, in the fiber links that are used to carry the mobile signals. We also investigated in chapter 5 the performance of such systems in the presence of noise that is introduced because of the fiber optics system. The performance of these links with respect to the changes in the input power or the modulation index was discussed.

In this chapter we shall explain the important concept of dynamic range of the mobile signals that reach the micro BS. We shall use the noise and nonlinear distortion results developed in the earlier chapters to determine the dynamic range for the system. This analysis will be performed for both the AMPS and the TDMA signals.

6.1 Dynamic range for the mobile signals

In cellular radio systems, the strength of the signal that is received at the base station changes constantly. If a mobile that is transmitting a signal to the base station is far away from the base station, then the power of the RF signal that is received at the base station from this mobile is weak. As the mobile starts approaching the base station, the strength of the received signal also increases. Also if the signal from the mobile experiences fading, then the power received at the base station can change. This situation is different from the CATV applications where all the signals that are transmitted over the fiber always have the same power.

Dynamic range can be defined as the total allowable variation of the input signal, such that noise and the nonlinear distortion degradation of the signal is within acceptable limits. Dynamic range can be interpreted in three ways.

1) Single signal dynamic range:

The power of the input signal is varied from the minimum possible value to the maximum possible value. As the signal starts getting stronger, it causes an increase in the modulation index (as can be seen from eqn 5.24). This increase in the modulation index causes an increase in the nonlinear distortion as was shown in both chapters 3 and 4. The maximum power to which the incoming signal can be increased is limited by the maximum allowable nonlinear distortion in the signal.

Now we start reducing the signal strength. As the input power decreases, as discussed in chapter 5, the signal to noise ratio decreases and, in a digital system, the bit error rate increases. The minimum power that can be received at the base station is limited by the minimum allowable signal to noise ratio in the AMPS standard and by the maximum allowable bit error rate in the TDMA standard.

The dynamic range of the system is the difference (in dB) between the maximum and the minimum allowable powers. This dynamic range is illustrated in Fig. 6.1. Thus the dynamic range is limited by the nonlinear distortion at one end and by noise at the other end.

The single signal dynamic range can be improved by preprocessing the signal such that the power variation at the output of the preprocessor is less than the variation at the input. Automatic gain control (AGC) is an example of such preprocessing.

2) Weak-Strong Dynamic Range:

This interpretation of the dynamic range is typical to the case of mobile radio signals. Consider the case of signals from three mobiles arriving at the base station at the same time. Of these signals, two of the signals are strong signals (at frequencies f_1 and f_2) and one signal is relatively weak (at frequency f_3). Also the weak signal lies at the frequency

of a third order intermodulation product of the two strong signals (i.e., $f_3 = 2f_1-f_2$ or $f_3 = 2f_2 - f_1$). Also let us assume that the weak signal is at the noise limit of the system and further noise degradation of this signal would cause unacceptable performance. Now the power of the strong signals is increased which causes a corresponding increase in the nonlinear intermodulation component at f3. The limit to which the strength of the strong signals can be increased is limited by the maximum allowable nonlinear distortion at the weak signal.

Then the weak-strong dynamic range of the system is the difference in the power of the weak signal and the maximum possible power of the strong signals.

In the absence of preprocessing, the weak strong dynamic range is equal to the single signal dynamic range if all the individual signals have equal strengths. This is true in CATV systems. However if the weak signal is weaker than the stronger signals by x dB then the weak strong dynamic range for the weak signal is lower than the single signal dynamic range by x dB. Thus, investigation of the single signal dynamic range also gives insight into the weak-strong dynamic range.

Unless the combined signal that is received at the micro BS is seperated into the individual channels before sending it over the fiber link, single signal dynamic range enhancing techniques like AGC cannot improve the weak strong dynamic range.

3) Spur Free Dynamic Range:

Let us consider Fig. 6.2 for the explanation of this dynamic range. The line 3 signifies the noise power in the signal. Line 2 is the power of the nonlinear distortion, while the line 1 is the power of the fundamental signal. Note that for a 3 dB increase of the input power, the third order nonlinear distortion power increases by 9 dB compared to a 3 dB increase in the fundamental output. The input power at which the fundamental power and the nonlinear distortion power are equal is called the third order intercept point (TOI). Now in this definition of the dynamic range the maximum allowable nonlinear distortion power is taken to be equal to the noise power. Then the spur free dynamic range of the signal is the difference between the fundamental power and the noise floor at that input power

when the nonlinear distortion is equal to the noise power [2,8,10]. It increases with the TOI of the laser.

The effective dynamic range of the system is the spur free dynamic range minus the required signal to noise ratio for the system.

The spur free dynamic range is equal to the single signal dynamic range if the maximum allowable nonlinear distortion in the single signal case is equal to the noise floor. The advantage of using the spur free dynamic range is that it can be easily determined from the noise floor and third order intercept point. But if the nonlinearity requirement is different from the noise requirement then the dynamic range should be expressed in terms of the single signal dynamic range rather than the spur free dynamic range.

From the above discussion, we saw that in the absence of preprocessing, the weak strong dynamic range can be determined from the single signal dynamic range. Also defining the dynamic range in terms of the single signal dynamic range is much more flexible to changes in the specifications of the standards than the spur free dynamic range. Hence, in this analysis we shall consider the single signal dynamic range.

6.3 Noise and Nonlinear Distortion Requirements for AMPS and TDMA systems

As can be seen from the above discussion, any interpretation of dynamic range depends on the specified requirements for the AMPS and the TDMA standards. The most important specifications for our application are the maximum nonlinear distortion allowed and the minimum signal to noise ratio (for AMPS) or the maximum BER (for TDMA).

For the AMPS standard, the system requirements for the noise and the nonlinearity are as follows

Minimum signal to noise ratio: 18 dB
Maximum Nonlinear Distortion: -70 dBc

For the TDMA standard, the system requirements are:

Maximum BER: 10^{-3}
Maximum Nonlinear Distortion: -70dBc

For the nonlinear distortion, we combine the nonlinearity obtained from the gain saturation and the dispersion and chirp and threshold clipping.

6.4 Dynamic Range results

In Fig. 6.3, we show the effects of gain saturation, dispersion and clipping and finally threshold clipping. We see that gain saturation and dispersion nonlinearities are comparable in magnitude. Also as discussed in chapter 2, when the modulation index crosses 5.5%, threshold clipping sets in. At this stage, clipping causes an extremely sharp degradation in the nonlinear performance, which has been indicated by a sharp drop in the fundamental to intermod ratio curve. The modulation index per channel at which clipping sets in is dependent on the number of channels that are in service. In Fig. 6.3 we have assumed the worst case of all 56 channels being operational.

The individual nonlinearities can be added as

$$\frac{I}{C}_{total} = \left(\left(\frac{I}{C}\right)_{dispt}^{0.5} + \left(\frac{I}{C}\right)_{clipt}^{0.5} + \left(\frac{I}{C}\right)_{gain\ satn}^{0.5} \right)^2 \qquad (6.1)$$

where I/C is the intermodulation to carrier ratio. The nonlinearities are additive in the optical power stage and since the photodetector converts optical power linearly into electrical current we use the square of the sum of the individual squareroots when considering electrical power.

Figure 6.4 shows the combined effect of nonlinearity when plotted as a function of the input power. As was discussed in chapter 5, the relation between the input power and the modulation index is

$$P_{in} = \left((I_B - I_{TH})m\right)^2 R_{laser} \qquad (6.2)$$

where m is the modulation index per channel, I_B is the bias current of the laser (= 40mA), I_{TH} is the threshold current of the laser (= 20mA) and R_{laser} is the input resistance of the laser (=50Ω).

For both the TDMA and the AMPS standards the maximum intermodulation interference is taken to be -70 dbc. Then as we can see from Fig. 6.4 the maximum input power can be -43 dBW. This is the upper limit for the input power. Any further increase in the power would cause unacceptable performance.

Figure 6.5 shows the noise performance of the AMPS signal when the background noise power spectral density is 10^{-10}W/Hz (which corresponds to a SNR at the output of the FM receiver of 22 dB in the absence of fiber link noise). We can see that the minimum input power required for maintaining a SNR of 18 dB is -106 dBW. Also from Fig. 6.6 at a power spectral density of 10^{-12}dB/Hz (which corresponds to a SNR of 42 dB in the absence of fiber noise) the minimum input power required is -107 dBW. Thus the dynamic range for power spectral density is 10^{-10}W/Hz is 63dB. This is the single signal dynamic range. Also the single signal dynamic range for the weaker background noise signal case where power spectral density is 10^{-12}W/Hz the dynamic range is 65dB. We see that due to stronger background noise, the dynamic range reduces in the first case. However we can also note that a 20 dB background noise reduction in Fig. 6.6 caused only a 2 dB increase in the dynamic range. This is because at the low input powers the fiber noise dominates over the background noise and hence the minimum input power required for maintaining stable noise performance is dependent more on the fiber introduced noise than on the background noise.

Now let us discuss the results for the TDMA signals. We see from Fig. 6.7 that in the case when the $C/N_{background}$ is 10dB, the minimum power required for a maximum BER of 10^{-3} is -109 dBW. Thus the single signal dynamic range in this case is 66 dB. In a less noisy environment when the $C/N_{background}$ is 20dB, the minimum power required is -111 dBW. Thus the dynamic range is 68 dB. This behavior is shown in Fig. 6.8. Again a strong improvement in the signal to noise ratio of the incoming signal does not cause any significant improvement in the dynamic range.

From the results for AMPS and TDMA signals, we see that the dynamic ranges for either case under equivalent conditions are comparable and show the same behavior with respect to the background noise and nonlinearity.

Also we see that the dynamic range is limited by the threshold clipping nonlinearity rather than by either the gain saturation or the dispersion nonlinearity. Thus as the number of active channels decreases, the threshold clipping sets in at a higher input power and dynamic range would consequently improve. This behavior is shown in Fig. 6.9 for the case of AMPS signals with power spectral density 10^{-12}W/Hz.

6.4 Summary

In this chapter, we discussed the concept of dynamic range for mobile signals. The combination of results from earlier chapters was then used to find the single signal dynamic range for both the AMPS and the TDMA mobile signals.

We discussed the behavior of the dynamic range in the presence of excess background noise. We saw that as the noise in the incoming signals increases, the dynamic range drops. We also saw that the dynamic range was limited by the threshold clipping. Consequently, as the number of active channels increases, the dynamic range reduces since clipping sets in at lower input powers.

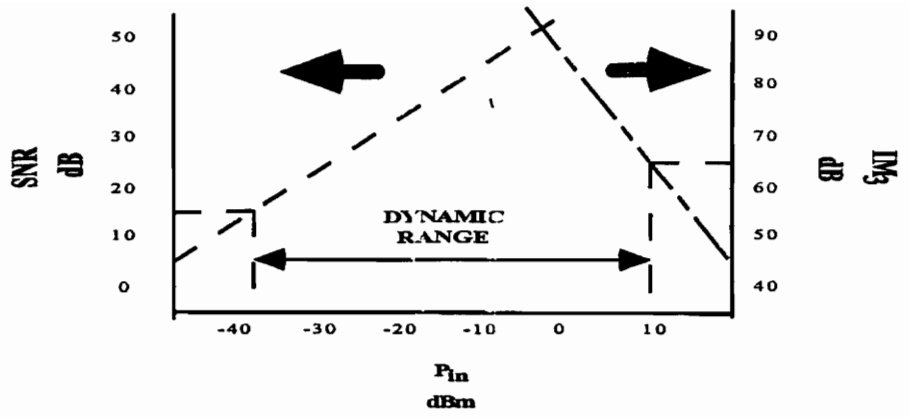

Fig. 6.1 Single Signal Dynamic Range

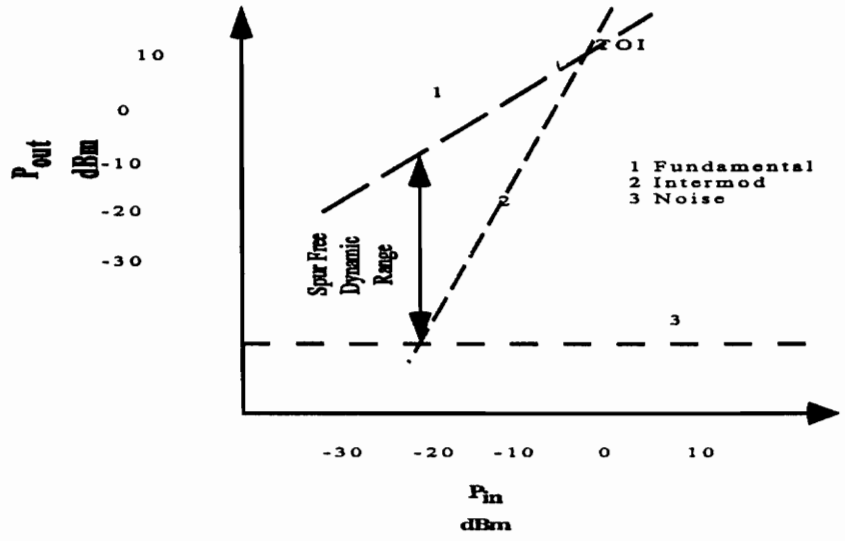

Fig. 6.2 Spur Free Dynamic Range

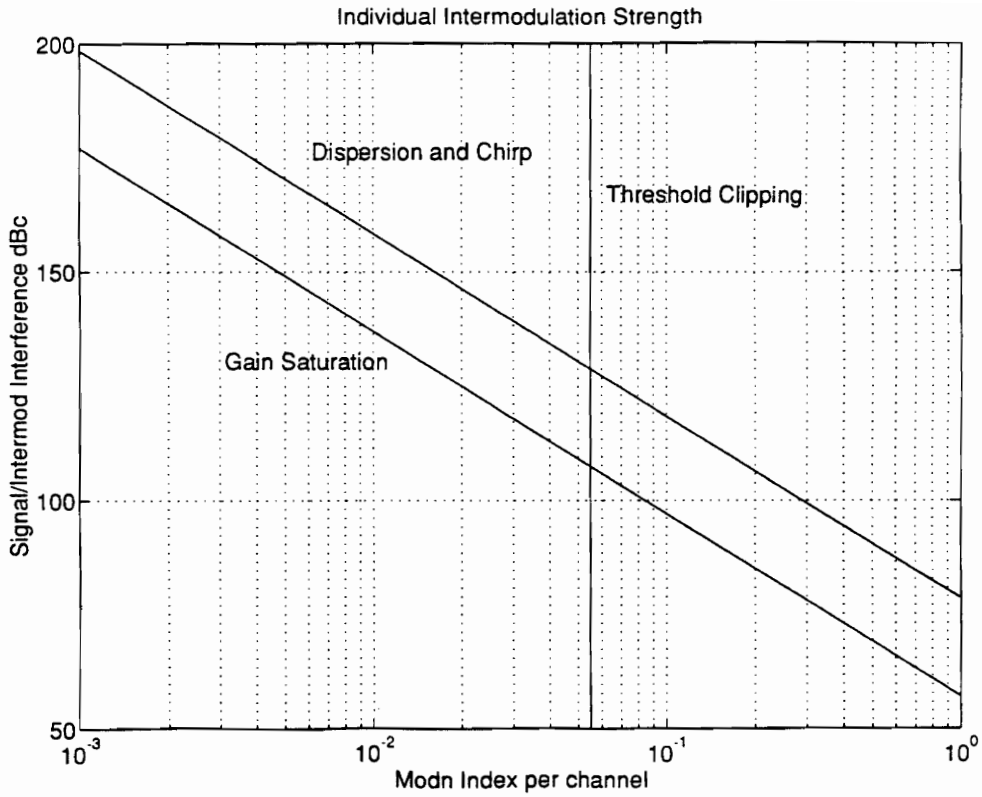

Figure 6.3 Effect of various nonlinearities versus modulation index

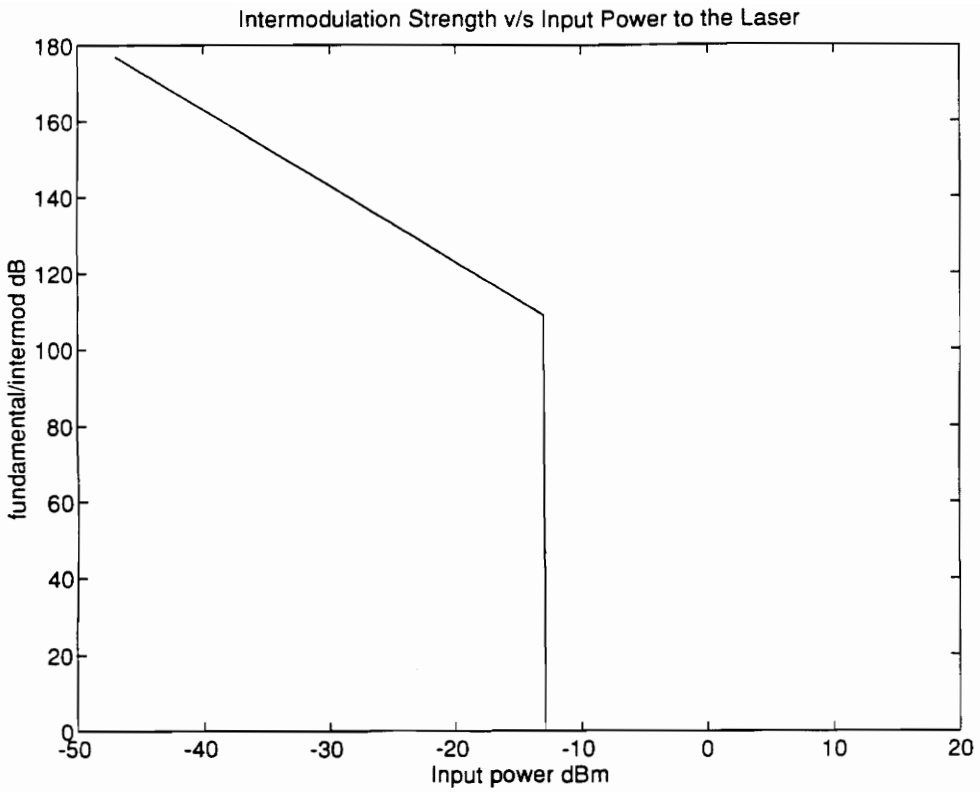

Figure 6.4 Combined nonlinearity versus input power (dBm)

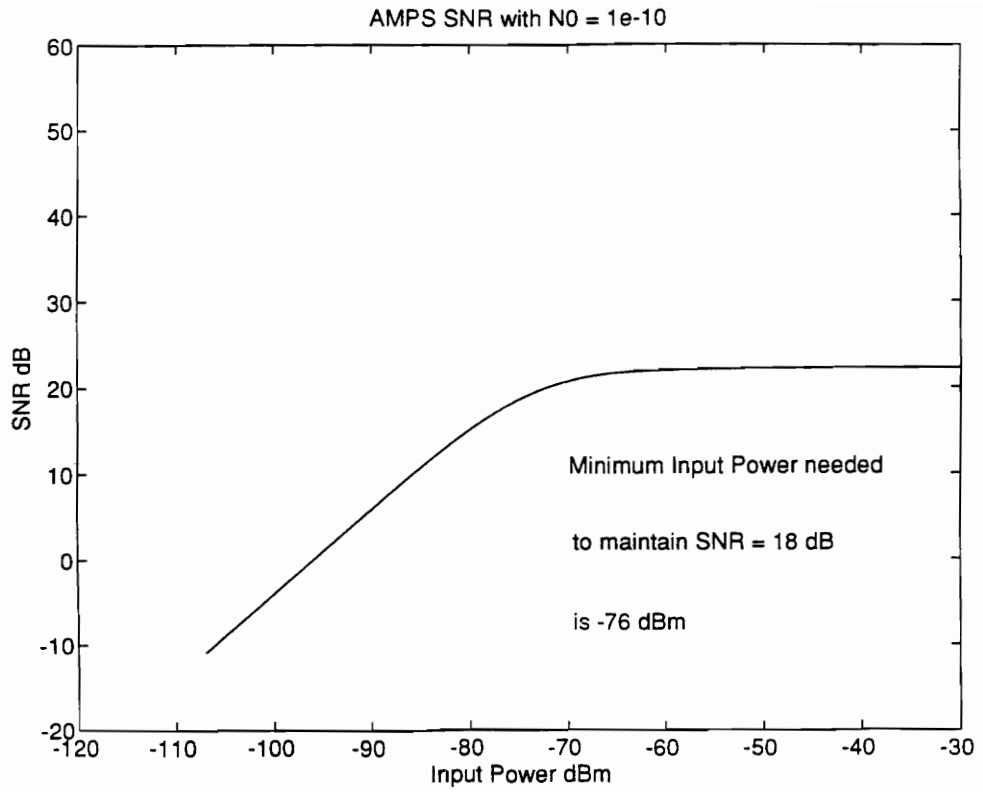

Figure 6.5 AMPS SNR variation with input power for $N_0 = 10^{-10}$

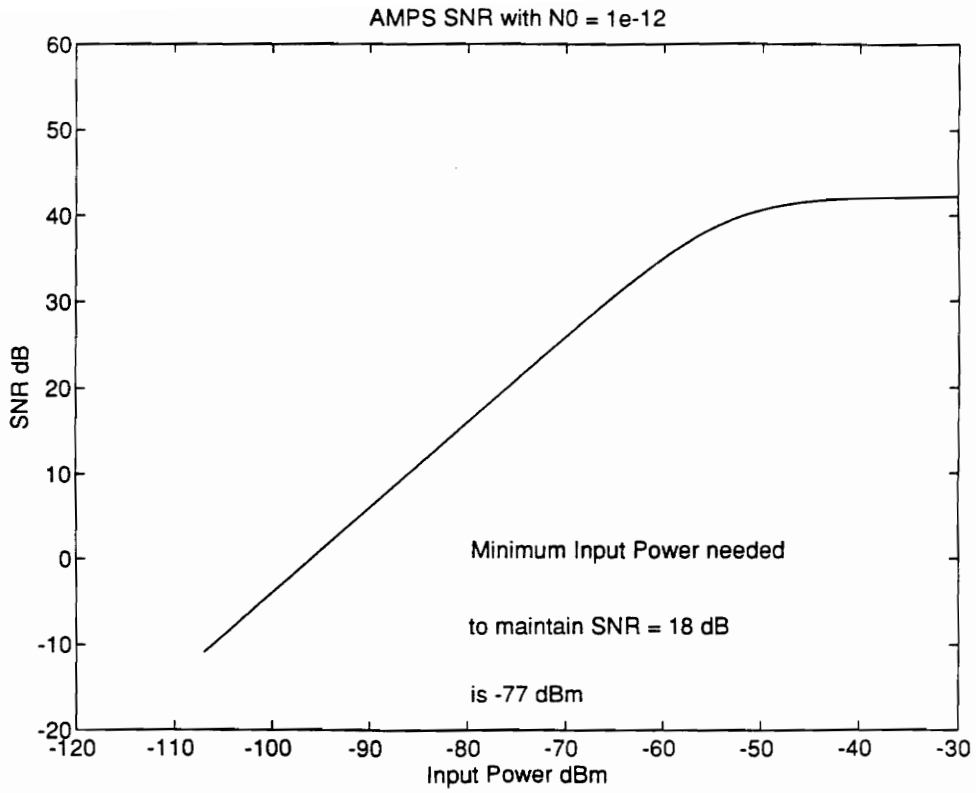

Figure 6.6 AMPS SNR variation with input power for $N_0 = 10^{-12}$

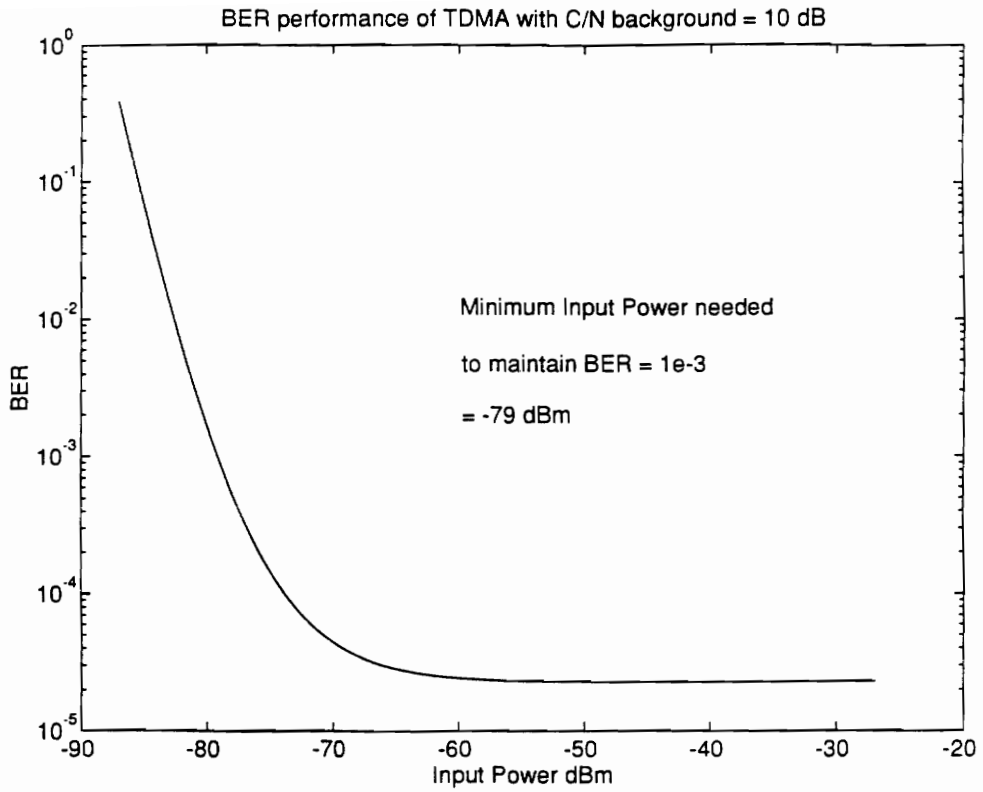

Figure 6.7 BER for TDMA variation with input power (dBm) for $CNR_{background}$ = 10 dB

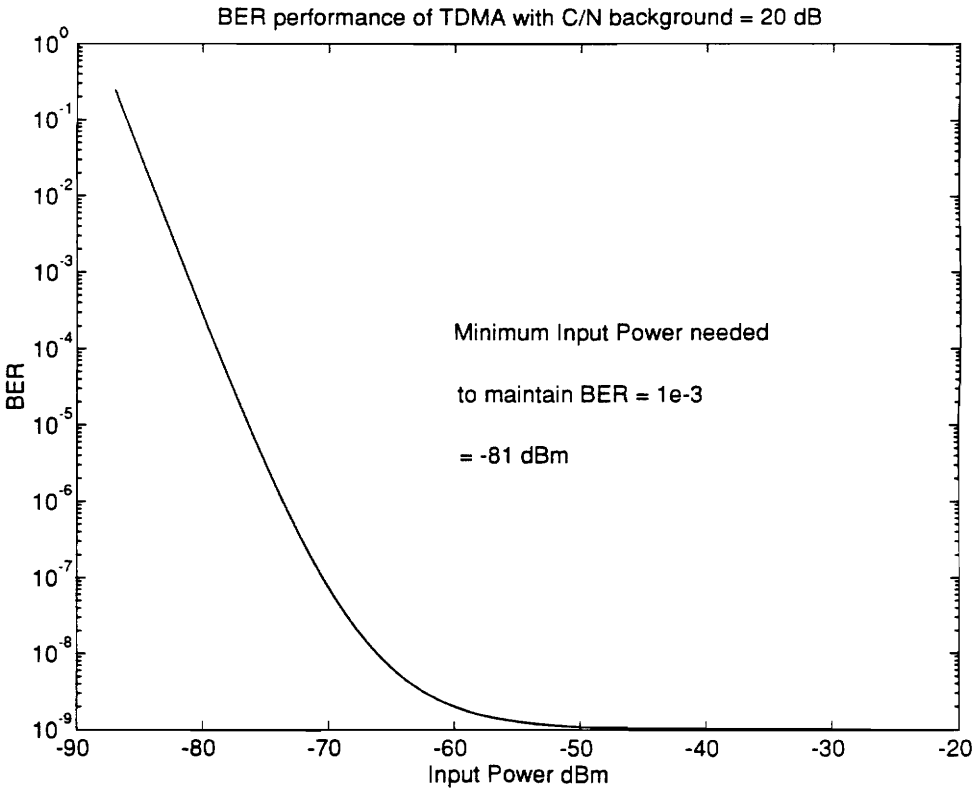

Figure 6.8 BER for TDMA variation with input power (dBm) for $CNR_{background}$ = 20 dB

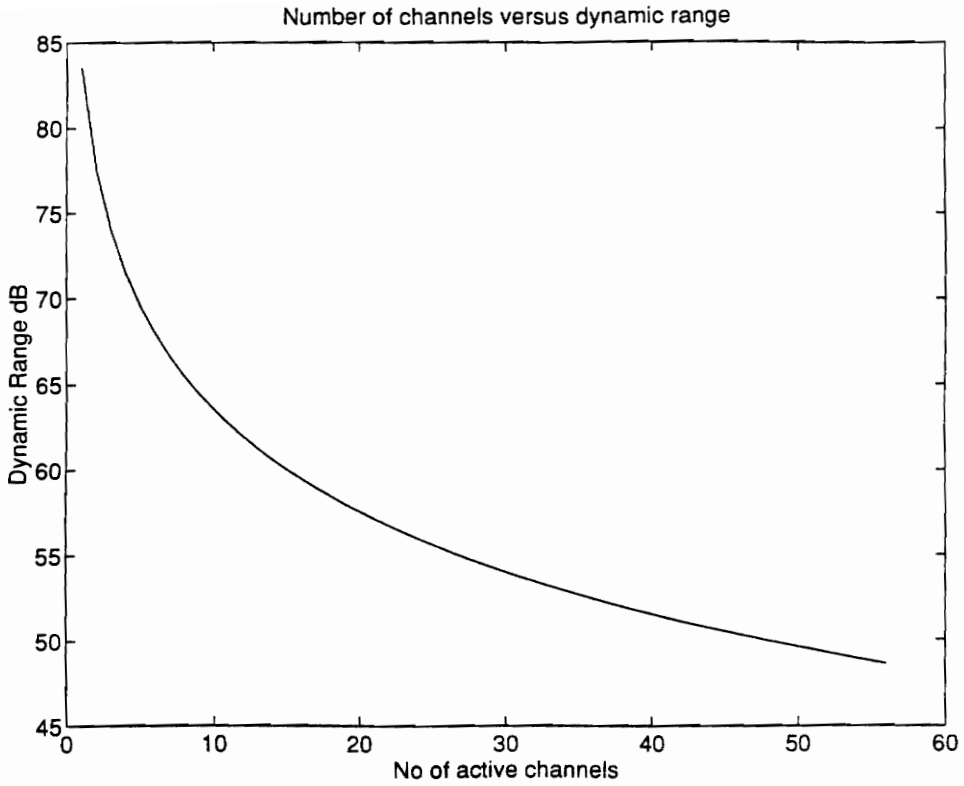

Figure 6.9 Dynamic range (dB) versus number of active channels

Chapter 7.

Summary and Conclusions

In this thesis, we investigated the dynamic range limitations caused by the noise and nonlinear distortion introduced because of the fiber. On the basis of the results obtained from the nonlinear distortion and noise study, the dynamic range for AMPS and TDMA signals were obtained.

The AM-SCM technique is used to transmit the signals received at a microcell base station to the central base station over fiber optic links. This scheme results in a simple and inexpensive architecture of the microcell base stations. But use of the fiber link also introduces noise and nonlinear distortion into the cellular mobile signals.

The major source of the nonlinearity was seen to be the third order intermodulation nonlinearity. We developed nonlinear models for gain saturation, combination of dispersion and chirp and threshold clipping. The gain saturation nonlinearity was found to be extremely dependent on the physical parameters of the laser. The behavior of the gain saturation nonlinearity with the modulating index per channel was investigated for several values of the gain saturation parameter ε. We also observed that the nonlinear distortion because of gain saturation increases as the frequency of the modulating input signal approaches the resonance frequency of the lasers. As the frequency of the cellular mobile signals (between 800 MHz and 900 MHz) is close to the resonance frequency of the lasers used for analog applications, the effect of gain saturation increases. Dispersion and chirp nonlinearity was found to be significant even though the length of the fiber used in the microcellular environment is less than 10 kms. However, threshold clipping limited the nonlinear performance of the system.

We also investigated the behavior of the AMPS and TDMA signals in the presence of fiber link noise. At low input power levels, the fiber link noise is dominant over the RF channel background noise. However, the best signal to noise ratio performance is limited by the RF channel noise. We also saw that the behavior of the signal to noise ratio in AMPS and the BER performance in TDMA signals is comparable in the absence of fading.

The concept of dynamic range was discussed in chapter 6. The minimum input power that must be received at the microcell base station is limited by the noise performance expected from the system. The nonlinear distortion limits the maximum input power that can be received at the microcell base station. The nonlinear analysis and the noise analysis was combined to analyze the dynamic range for AMPS and TDMA signals without any signal level preprocessing. The nonlinear distortion is limited by the threshold clipping nonlinearity. The minimum input power required is limited by the noise introduced by the fiber link. We also investigated the variation of the dynamic range for AMPS signal with the number of active channels that are received at the microcell base station.

Future Work

Considerable research is being focussed on dynamic range enhancing range techniques for the fiber link in mobile radio systems. The dynamic range enhancing techniques proposed can be classified into optical techniques and electrical techniques. The optical methods include RIN noise cancellation, use of polarizartion combining techniques and use of multiple laser diodes. These techniques reduce the noise or nonlinearity that is introduced by the fiber link and thus increase the dynamic range. The electrical techniques for dynamic range enhancement include automatic gain control (AGC), predistortion and companding. The goal of using these methods is to reduce the signal magnitude so that the nonlinearity introduced by the fiber link is minimal. Some techniques like FM double modulation make use of both techniques. A further study of these techniques using the nonlinear and noise models developed in this thesis could lead to a much better understanding of the fiber link and improvement of the dynamic range performance.

REFERENCES

[1] G. P. Agrawal, Fiber Optic Communication Systems, John Wiley and Sons, Inc., 1992.

[2] D. M. Fye, " Design of fiber optic antenna remoting links for cellular radio applications," *Proceedings of VTC'90*, pp 622-625, May 1990.

[3] M. Shibutani, T. Kanai, W. Domom, K. Emura, and J. Namiki, " Optical fiber feeder for microcellular mobile communications systems,"*IEEE J. Select. Areas in Comm.*, vol. 11, no. 7, pp 1118-1126, 1993.

[4] D. Chan and T. M. Yuen, " System analysis and design of a fiber optic VSB-FDM system for video trunking," *IEEE Trans. Commun.*, vol. COM-25, no. 8, pp 680-689, 1977.

[5] T. E. Darcie, M. E. Dixon, B. L. Kasper and C. A. Burrus, " Lightwave systems using microwave subcarrier multiplexing," *Electron. Lett.*, vol. 22, pp. 774-775, 1986.

[6] R. Olshansky, V. A. Lanzisera, " 60-channel FM video subcarrier multiplexed optical communication system," *Elect. Lett.*, vol. 23, p. 1196, 1987.

[7] J. A. Chiddix and W. S. Chiciora, " Introduction of optical fiber transmission technology into existing cable television networks and its impact on the consumer electronics interface," *IEEE Trans. Consumer Electron.*, no. 5, pp 51-62, May 1989.

[8] W. E. Stevens, T. R. Joseph, " A 1.3μm microwave fiber optic link using a directly modulated laser transmitter," *J. Lightwave Technol.*, vol LT-3, no. 2, pp 308-315, 1985.

[9] K. Morita and H. Ohtsuka, " The new generation of wireless communications based on fiber-video technology," *IEICE Trans. Commun.*, vol. E76-B, no. 9, pp 1061-1068, September 1993.

[10] W. I. Way, "Optical fiber based microcellular systems: an overview," *IEICE Trans. Commun.*, vol E76-B, no. 9, pp 1091-1099, 1993.

[11] R. Ohmoto, H. Ohtsuka, and H. Ichikawa, "Fiber optic microcell radio systems with a spectrum delivery scheme", *IEEE J. Select. Areas in Comm.*, vol 11, no. 7, pp1108-1117, 1993.

[12] M. Shibutani, W. Domon and K. Emura, " Performance improvement in optical fiber feeders for microcellular mobile radio systems," *IEICE Trans. Commun.*, vol. E76-B, no. 9, pp 1145-1151, 1993.

[13] T. Okuno, H. Mizuguti, S. Komaki and N. Morigana, " A new frequency switching/ IM3 reduction method in fiber optic technology," *IEICE Trans. Commun.*, vol. E76-B, no. 9, pp 1178-1185, 1993.

[14] L. M. Johnson and H. V. Roussell, " Linearization of an interferometric modulator at microwave frequencies by polarization mixing," *IEEE Photon. Technol.* Lett., vol. 1, no. 11, pp 810-811, Nov. 1990.

[15] S. K. Korotky and R. M. Defidder, " Dual parallel modulation schemes for low distortion analog optical transmission," *IEEE J. Select. Areas Commun.*, vol. 8, no. 7, pp 1377-1381, September 1990.

[16] M. I. Farewell, I. Q. Lin, E. Wooten and W. S. C. Chang, " An electrooptic intensity modulator with improved linearity," *IEEE Photon. Technol. Lett.*, vol. 3, no. 9, pp 792-795, September 1991.

[17] J. H. Schaffner and W. B. Bridges, " Intermodulation distortion in high dynamic range microwave fiber-optic links with linearized modulators," *J. Lightwave Technol.*, vol. 11, no. 1, 1993.

[18] C. Y. Kuo, " Fundamental nonlinear distortions in analog links with fiber amplifiers," *J. Lightwave Technol.*, vol. 11, no. 1, pp 7-15, 1993.

[19] K. Y. Lau, A. Yariv, " Intermodulation distortion in a directly modulated semiconductor injection laser," *Appl. Phys. Lett.*, vol 45 no 10, pp 1034-1036, 1984.

[20] W. I. Way, " Large signal nonlinear distortion prediction for a single mode laser diode under microwave intensity modulation," *J. Lightwave Tecnol.*, vol LT-5 no. 3, pp 305-315, 1987.

[21] T. E. Darcie, R. S. Tucker, G. J. Sullivan, " Intermodulation and harmonic distortion in InGaAsP lasers," *Electron. Lett.*, vol 21 no. 16, pp 665-666, 1985.

[22] A. A. M. Saleh, " Fundamental limit on number of channels in SCM lightwave CATV system," *Electron. Lett.*, vol 27, no. 14, pp 776-777, 1989.

[23] C. J. Chung and Ira Jacobs, " Practical TV channel capacity of lightwave multichannel AM SCM systems limited by the threshold nonlinearity of laser diode," *IEEE Photonics Technol. Lett.*, vol 4, no 3, pp 289-292 1992.

[24] E. E. Bergmann, C. Y. Kuo, and S. Y. Huang, " Dispersion induced composite second-order distortion at 1.5μm", *IEEE Photonics Technol. Lett.*, vol. 3, no. 1, pp 59-61, 1991.

[25] A. R. Chraplyvy, " Limitations on lightwave communications imposed by optical fiber nonlinearities", *J. Lightwave Technol.*, vol. 8, no. 10, pp 1548-1557, 1990.

[26] X. P. Mao, G. E. Bodeep, R. W. Tkach, A. R. Chraplyvy, T. E. Darcie, and R. M. Derosier, " Brillouin scattering in externally modulated lightwave AM-VSB CATV transmission systems", *IEEE Photonics Technol. Lett.*, vol 4, no. 3, pp 287-483, 1992.

[27] S. E. Miller, I. P. Kaminow, Optical Fiber Telecommunications II, Academic Press, 1988.

[28] Leon Couch, Digital and Analog Communications Systems, Macmillan: London, 1990.

[29] A. A. M. Saleh and L. J. Cimini Jr., " Indoor radio communications using Time Division Multiple Access with cylindrical slow frequency hopping and coding," *IEEE J. Select. Areas Commun.*, vol. 7, jno. 1, pp 59-70, Jan 1989.

VITA

Anish S. Kelkar was born in Woodbury, NJ on October 1, 1971. He left America with his parents in 1973 and studied in India till his undergraduate degree. He received his undergraduate degree in Electronics Engineering from the Victoria Jubilee Technical Institute, Bombay, India in July 1992. He then joined the graduate program in Electrical Engineering at Virginia Tech. In the summer of 1993, he worked as a Summer Intern in the GSM Hardware Department of AT&T Bell Laboratories, Whippany, NJ. Anish Kelkar received his Masters degree in November 1994.

His research interests include cellular communications and analog transmission on fiber optic links.

A S. Kelkar